energies

MDPI

Article

A Stochastic MILP Framework for Risk-Aware and Degradation-Conscious Energy Management in Residential Multi-Home Systems

Adool Kruekaew [1], Ariya Namvong [1], Manussawee Nokkaew [1], Chayada Surawanitkun [1,*], Nuttapong Bootthanu [2], Narong Amorntep [3,*] and Apirat Siritaratiwat [4]

[1] Center of Multidisciplinary Innovation Network Talent (MINT Center), Faculty of Interdisciplinary Studies, Khon Kaen University, Nong Khai Campus, Nong Khai 43000, Thailand; kadool@kkumail.com (A.K.); ariyna@kku.ac.th (A.N.); manuno@kku.ac.th (M.N.)
[2] Department of Smart Electronics and Electric Vehicles, Faculty of Technology and Engineering, Udon Thani Rajabhat University, Udon Thani 41000, Thailand; nuttapong.bo@udru.ac.th
[3] Department of Electronics Technology, Faculty of Science, Ramkhamhaeng University, Bangkok 10240, Thailand
[4] Department of IoT and Information Engineering, School of Engineering, King Mongkut's Institute of Technology, Ladkrabang, Bangkok 10520, Thailand; apirat.si@kmitl.ac.th
* Correspondence: chaysu@kku.ac.th (C.S.); narong.a@rumail.ru.ac.th (N.A.)

Abstract

The integration of photovoltaic (PV) systems, energy storage systems (ESSs), and electric vehicles (EVs) in residential communities introduces challenges from renewable-generation uncertainty, load variability, and battery degradation. This paper proposes a stochastic mixed-integer linear programming (MILP) framework for centralized multi-home energy management with aggregated PV and ESS resources and household EVs. The framework minimizes expected electricity cost while controlling operational risk, quantified by Conditional Value-at-Risk (CVaR), and shared-ESS cycling-related degradation, represented by the equivalent full cycle (EFC) metric. An ε-constraint formulation with a causal-adaptive ESS dispatch coordinates these requirements, and static and adaptive strategies are evaluated on independent test scenarios. For the 10-home case, the proposed strategy reduces expected cost by 0.24%, $CVaR_{0.90}$ by 2.18%, and ESS EFC by 4.37% relative to the static baseline. Relative to the adaptive baseline, it reduces ESS EFC by 4.46% for a 1.12% cost increase, with a practically unchanged $CVaR_{0.90}$ and no increase in EV throughput; the CVaR reduction arises mainly from the adaptive recourse. Scalability tests with up to 50 households confirm computational practicality for 24 h day-ahead scheduling.

Keywords: home energy management system; stochastic mixed-integer linear programming; Conditional Value-at-Risk; equivalent full cycle; electric vehicle

Check for updates

Academic Editor: Michael Short

Received: 23 September 2026
Revised: 26 October 2026
Accepted: 28 October 2026
Published: 2 November 2026

Copyright: © 2026 by the authors. Licensee MDPI, Basel, Switzerland. This article is an open access article distributed under the terms and conditions of the Creative Commons Attribution (CC BY) license.

1. Introduction

Home energy management systems (HEMSs) coordinate residential demand and distribute energy resources, as demonstrated by a hierarchical framework for managing photovoltaic (PV) systems, energy storage systems (ESSs), and bidirectional electric vehicle (EV) operation [1]. A demand-side management framework was developed to schedule household appliances, PV generation, ESS operation, and EV charging under day-ahead electricity pricing [2]. A residential load-shifting model was formulated to balance electricity cost reduction with user discomfort [3]. Researchers then developed a multi-objective real-time HEMS to minimize electricity cost while reducing visual and thermal discomfort [4].

As residential energy resources became increasingly integrated, a mixed-integer linear programming (MILP)-based scheduling framework was proposed for both single-home and centralized multi-home systems under real-time electricity pricing [5]. Vehicle-to-Home (V2H) operation was incorporated into residential energy management to enable EV batteries to support household demand [6]. Multi-objective scheduling of PV, ESS, and EV resources was employed to minimize electricity cost, peak-to-average ratio, and wasted PV energy [7]. Learning-based approaches have further improved real-time adaptability through soft actor-critic reinforcement learning [8], adaptive dynamic programming [9], data-driven deep reinforcement learning (DRL) under uncertain household conditions [10], and hybrid mathematical optimization-reinforcement learning [11]. Although these studies improve residential scheduling, most focus on economic performance, user comfort, or adaptive control without jointly addressing operational risk and battery degradation.

Research has subsequently expanded from individual homes to multi-home and community energy management. Distributed transactive coordination was used to accommodate household cost, comfort, and privacy preferences in residential communities [12]. A neighborhood energy-storage community model coordinated household appliances, EV charging, and storage batteries to improve grid operation [13]. Researchers evaluated the technical and economic feasibility of community-scale PV, ESS, EV charging, V2H, and transactive energy management [14]. Peer-to-peer energy trading among residential prosumers was investigated through the coordinated operation of responsive demand and distributed energy resources [15]. Community demand response using ESSs and EVs was developed to support peak shaving and coordinated load scheduling [16]. Coordinated EV-fleet charging strategies were compared for demand response in solar-powered building communities [17]. A neighborhood framework incorporated household PV systems, a shared ESS, an EV fleet, uncertain EV behavior, demand response, and battery degradation cost [18]. Distributed coordination between EV charging stations and HEMSs was proposed to reduce neighborhood costs and smooth aggregated demand [19]. Real-time multi-home scheduling using multi-agent DRL was developed to coordinate energy trading and EV charging among residential prosumers [20]. However, integrated risk and degradation management remains limited in multi-home energy systems.

Uncertainty in PV generation, residential demand, electricity prices, and EV availability can substantially affect the feasibility and economic performance of residential energy schedules. Multi-uncertainty ESS sizing and energy management for smart-home communities were investigated by considering market prices, PV generation, EV charge levels, and grid conditions [21]. A stochastic MILP model used representative electricity prices and solar-irradiance scenarios for appliance, PV, and battery scheduling [22]. A robust multi-objective HEMS was developed to account for uncertainty in PV generation, electricity tariffs, and appliance operating durations [23]. A two-stage robust optimization framework was proposed to integrate PV-battery storage, EV charging, and demand response under uncertain operating conditions [24]. Appliance scheduling was evaluated under uncertain EV and renewable-generation conditions to reduce electricity cost and grid dependency [25]. Although these approaches improve scheduling robustness, ensuring feasible operation under uncertainty does not directly quantify the economic severity of unfavorable tail scenarios. Conditional Value-at-Risk (CVaR)-based optimization was introduced into HEMS self-scheduling to manage electricity cost, peak-period energy purchases, and user discomfort [26]. Distributionally robust CVaR constraints were formulated to quantify microgrid power-balance risk under renewable-generation uncertainty [27]. Worst-CVaR optimization was developed to manage operational-cost risk under uncertain PV generation and multi-energy demand [28]. Wasserstein distributionally robust optimization and CVaR-constrained model-predictive control were combined to balance microgrid

cost and resilience [29]. Although these approaches demonstrate the value of risk-aware scheduling, battery degradation is generally excluded from their risk formulations.

Battery degradation is an important operational concern because intensive charging and discharging can shorten battery lifetime and increase long-term replacement costs. Battery lifetime was considered in the optimal sizing of residential PV-ESSs with EV integration [30]. EV battery capacity loss was estimated in a model-predictive HEMS using real-life annual data [31]. Battery discharging cycles were incorporated as a criterion in multi-objective residential energy management [32]. PV and ESS lifecycle costs were incorporated into appliance scheduling and energy-flow management [33]. Static and scenario-based dynamic models were developed to balance operating cost, user inconvenience, and storage-system durability [34]. A degradation-aware MILP formulation explicitly modeled battery cycle aging and the effects of different operating patterns [35]. However, these studies do not integrate CVaR-based tail-risk management with EFC-based ESS cycling-related degradation mitigation for centralized multi-home communities. Consequently, a research gap remains in coordinating aggregated community PV and ESS resources together with household EVs under uncertainty while balancing expected operating cost, adverse-scenario risk, and ESS cycling across different community sizes.

To address this research gap, this paper proposes a stochastic MILP framework for multi-home communities possessing equivalent aggregated PV and ESS resources with household EVs. The main contributions are as follows:

1. A unified stochastic MILP framework coordinates aggregated PV and ESS resources with household EVs under PV and load uncertainties.
2. CVaR-based risk management and EFC-based shared-ESS cycling control are integrated to limit adverse operating-cost scenarios and excessive ESS cycling.
3. An ε-constraint formulation with a causal-adaptive ESS dispatch coordinates expected operating cost, tail risk, and ESS cycling, enabling the proposed (CVaR+EFC) strategy, hereafter proposed, to minimize ESS cycling within a cost budget at practically unchanged tail risk and EV throughput.
4. The framework is validated against a published benchmark and evaluated on independent test scenarios, including degradation-inclusive cost, with sensitivity and scalability analyses for communities of up to 50 homes.

The remainder of this paper is organized as follows. Section 2 describes the system and dataset preparation. Section 3 presents the proposed stochastic MILP-based energy management framework. Section 4 discusses the results and key findings. Finally, Section 5 concludes the paper.

2. System Description and Dataset Preparation

2.1. Multi-Home Community Architecture

This study considers a centralized multi-home EMS comprising residential loads, household EVs, and equivalent aggregated PV and ESS resources. As illustrated in Figure 1, each household is physically equipped with rooftop PV panels and an ESS, while the central EMS coordinates these distributed resources through their equivalent aggregated representation. Thus, the aggregated PV and ESS are modeling equivalents rather than physically centralized community assets.

The capacities of the equivalent shared PV and ESS resources are scaled with the number of participating households; the per-home and aggregated values for the 10-home main case are given in Section 2.3.

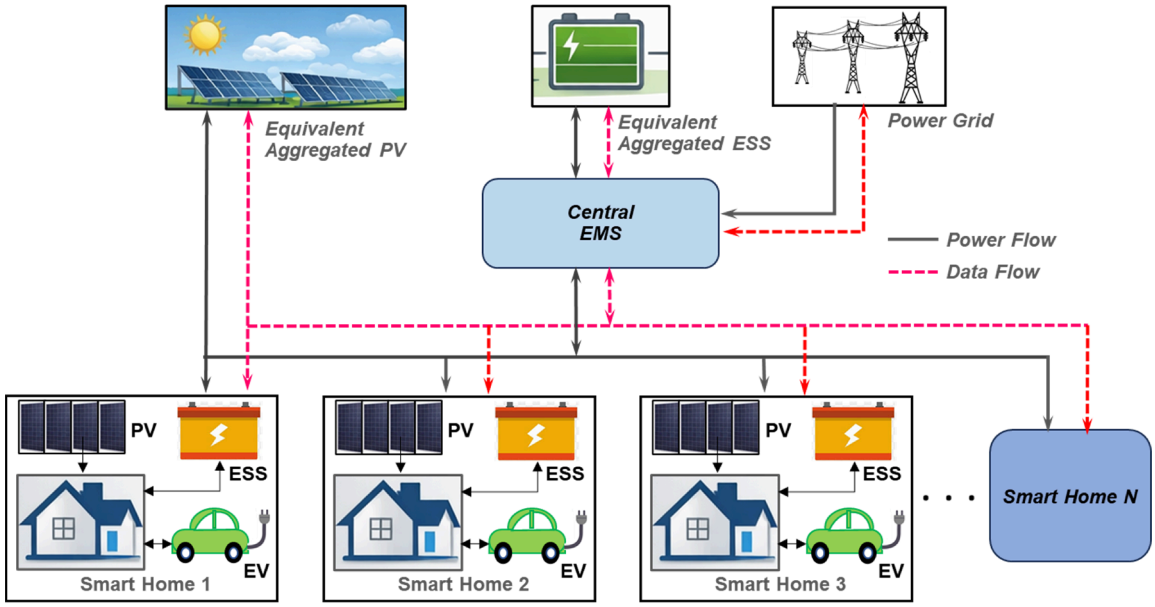


Figure 1. Proposed architecture of a multi-home community energy management system.

2.2. Community Dataset

The deterministic 3-home benchmark reported in [5] is used for model verification. For community-level analysis, residential demand data are obtained from the measured household dataset reported in [36]. The measured profiles of ten households (SH1–SH10), scaled to a common daily energy to prepare the data for the simulation, are used for the 10-home main case, while subsets are used for smaller community cases. For the 20- and 50-home scalability cases, additional household profiles are synthetically generated from the measured SH1–SH10 profiles. These larger cases are used only for the scalability analysis (Section 4.6).

The 10-home system constitutes the main-case study. The community configurations are summarized in Table 1. Figure 2 presents the aggregated residential load, shared PV generation, and real-time pricing (RTP) tariff used for the 10-home main case.

Table 1. Community dataset configuration used in this study.

Community Size	Data Source	Purpose
3 Homes	Published 3-home benchmark	Model verification
5 Homes	Subset of measured SH1–SH10	Intermediate evaluation
10 Homes	Measured SH1–SH10 profiles	Main-case study
20 Homes	Measured SH1–SH10 with synthetic extension	Scalability analysis
50 Homes	Measured SH1–SH10 with synthetic extension	Scalability analysis

2.3. System Parameters

Table 2 summarizes the principal system and stochastic optimization parameters. Each home is equipped with a 5 kW PV system and a 10 kWh ESS with a 2.5 kW power rating. The shared ESS operates within a 20–80% SOC range, with both the initial and terminal SOC fixed at 50%. The equivalent PV and ESS capacities are scaled according to the number of participating homes. One hundred stochastic training scenarios are considered for both the main-case and scalability analyses, with the CVaR confidence level set to 0.90; the strategies are evaluated on independent test scenarios (Section 2.5).

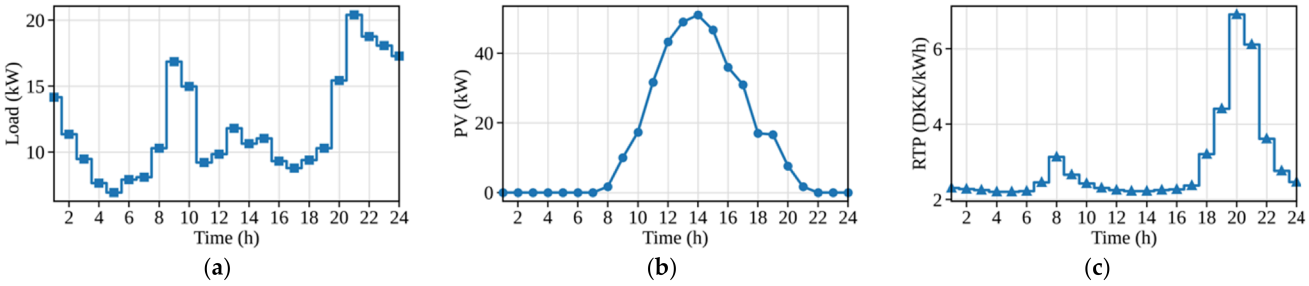


Figure 2. Input datasets used in the proposed EMS: (**a**) aggregated residential load, (**b**) aggregated shared PV generation, and (**c**) real-time pricing (RTP).

Table 2. System parameters and stochastic optimization settings.

Parameter	Value
PV capacity per home	5 kW
Equivalent aggregated PV capacity (10-home case)	50 kW
ESS energy capacity per home	10 kWh
Equivalent aggregated ESS capacity (10-home case)	100 kWh
ESS power rating per home	2.5 kW
Equivalent aggregated ESS power rating (10-home case)	25 kW
ESS charging/discharging efficiency	0.9
ESS SOC range	20–80%
EV SOC range (all EVs)	20–100%
Initial/final ESS SOC (main study)	50/50%
Training scenarios	100
Independent test scenarios	5 × 5000
CVaR confidence level (α)	0.90

2.4. EV Specifications

The EV specifications adopted in the 10-home main case are summarized in Table 3. The EV fleet includes different battery capacities, charging/discharging power ratings, arrival and departure times, and SOC conditions. These parameters define EV availability and feasible charging as well as V2H operation within the optimization model. EVs are not connected during roughly 09:00–17:00 (Table 3), so midday PV surplus can be absorbed only by the shared ESS.

The EVs participate in energy scheduling through controlled charging and V2H operation subject to their power, availability, and SOC constraints.

Table 3. Specifications of the 10 electric vehicles [36].

EV	Model	Capacity (kWh)	P^{ch} (kW)	P^{dis} (kW)	Efficiency (%)	t_{arr}	SOC_{arr} (%)	t_{dep}	SOC_{dep} (%)
EV1	Tesla Model S	60	11	11	90	19:00	50	08:00	80
EV2	Peugeot	50	7.4	7.4	90	17:00	60	09:00	80
EV3	Toyota RAV4 EV	40	10	10	90	20:00	40	06:00	80
EV4	Renault Fluence Z.E. 2011	22	3.5	3.5	90	18:00	50	07:00	80
EV5	Renault Zoe 2013	22	3	3	90	18:00	55	08:00	80
EV6	Tesla Model S 85 kWh 2013	85	22	22	90	19:00	50	07:00	80
EV7	Fiat 500e	24	3.3	3.3	90	17:00	60	09:00	80
EV8	Ford Focus Electric	23	6.6	6.6	90	20:00	45	08:00	80
EV9	Nissan Leaf	24	6.6	6.6	90	18:00	50	07:00	80
EV10	Chevrolet Spark EV 2014	21	3.3	3.3	90	19:00	55	09:00	80

2.5. Uncertainty Scenario Generation

Uncertainty in residential electricity demand and PV generation is represented using correlated stochastic scenarios. The nominal hourly load and PV profiles are used as the basis for scenario generation, while daily and temporally correlated variations are introduced over a 24 h scheduling horizon. This formulation preserves temporal dependence between consecutive hours and incorporates both community-wide and household-specific variations in residential demand. For PV generation, the scenario-dependent profile is expressed as

$$P_{s,t}^{PV} = P_t^{PV,0}\left(1 + \delta_s^{PV} + \xi_{s,t}^{PV}\right) \tag{1}$$

where $P_t^{PV,0}$ is the nominal aggregated PV generation at time t, δ_s^{PV} represents the scenario-dependent daily weather variation, and $\xi_{s,t}^{PV}$ represents the temporally correlated hourly variation. The daily PV component follows a zero-mean normal distribution with a standard deviation of 0.10, while the hourly component has a stationary standard deviation of 0.10. The resulting PV uncertainty multiplier is bounded between 0.20 and 1.35, and PV generation is further limited by the installed aggregated PV capacity.

The nominal demand of each household corresponds to its representative hourly profile derived from the measured load data described in Section 2.2. The scenario-dependent load of household h is expressed as

$$P_{h,s,t}^{L} = P_{h,t}^{L,0}\left(1 + \delta_s^{L} + \xi_{s,t}^{L} + \omega_{h,s,t}^{L}\right) \tag{2}$$

where $P_{h,t}^{L,0}$ is the nominal electricity demand of household h, δ_s^L represents the common daily demand variation, $\xi_{s,t}^L$ is the common temporally correlated hourly variation, and $\omega_{h,s,t}^L$ represents the household-specific residual variation. The daily load component follows a zero-mean normal distribution with a standard deviation of 0.05, while the household-specific residual has a standard deviation of 0.04. The common hourly load component has a stationary standard deviation of 0.06. The resulting load uncertainty multiplier is bounded between 0.65 and 1.40. The temporally correlated hourly variations in both PV generation and residential demand are modeled using a first-order autoregressive (AR(1)) process:

$$\xi_{s,t} = \rho\, \xi_{s,t-1} + \nu_{s,t} \tag{3}$$

where $\rho = 0.75$ is the temporal correlation coefficient and $\nu_{s,t}$ is a zero-mean Gaussian innovation term.

One hundred equiprobable training scenarios are generated using a fixed random seed of 42 for reproducibility; seeds 1042 and 2042 give two additional training sets. The same training set is used to optimize all strategies of Section 3.8 in the 10-home main case. All strategies are then evaluated on five independent test sets of 5000 scenarios each (seeds 10,001–10,005); smaller test sets used in the sensitivity analyses are described in Section 4.2. The RTP tariff remains deterministic across all scenarios. The resulting scenario-dependent operating costs are used to evaluate the expected operating cost and CVaR at the 90% confidence level, the CVaR being the mean cost of the worst 10% of the scenarios of a test set.

3. Stochastic MILP-Based Energy Management Framework

3.1. Stochastic Optimization Framework

The community EMS is formulated as a two-stage stochastic MILP model over a 24 h horizon with a 1 h resolution (interval t covers the clock time from $t-1$ to t, and energy states are defined at the end of an interval; the hour labels in figures and tables are the interval index t). PV generation and residential demand uncertainties are represented by the scenario set S described in Section 2.5. The shared ESS and EV charging/discharging schedules are

treated as day-ahead decisions and remain identical across scenarios in the static family. In the adaptive family, only the EV schedules do, and the ESS set-point responds causally to the deviations observed in the preceding hours (Section 3.9), whereas grid import and PV curtailment are scenario-dependent recourse variables. The non-anticipativity condition for a generic day-ahead variable $x_{s,t}$ is expressed as

$$x_{s,t} = x_{s',t},\ \forall s, s' \in S,\ t \in T \tag{4}$$

where T and S denote the sets of time intervals and uncertainty scenarios, respectively. It applies to the EV variables and, in the static family, to the ESS variables. All strategies use the same stochastic model and operational constraints but differ in their risk and ESS-cycling requirements and in the ESS dispatch rule, as formulated in the following subsections.

3.2. Expected Operating Cost

The operating cost under scenario s is determined by the hourly grid-import power and the corresponding RTP tariff:

$$C_s = \sum_{t \in T} \lambda_t P_{s,t}^{grid} \Delta t \tag{5}$$

where C_s is the operating cost under scenario s, λt is the RTP tariff, $P_{s,t}^{grid}$ is the grid-import power, and Δt is the scheduling interval. For Ns equiprobable scenarios, the expected operating cost is given by

$$\overline{C} = \frac{1}{N_s} \sum_{s \in S} C_s \tag{6}$$

The scheduling problem minimizes the expected operating cost as

$$\min \overline{C} \tag{7}$$

3.3. Community Power Balance

For each scenario and scheduling interval, the community power balance is maintained by coordinating PV generation, grid import, the shared ESS, and household EVs. Let H denote the set of households, with $h \in H$ representing the household index. The power balance is expressed as

$$\begin{aligned} &P_{s,t}^{PV} + P_{s,t}^{grid} + P_{s,t}^{ESS,dis} + \sum_{h \in H} P_{h,s,t}^{EV,dis} \\ &= P_{s,t}^{L} + P_{s,t}^{ESS,ch} + \sum_{h \in H} P_{h,s,t}^{EV,ch} + P_{s,t}^{curt},\ \forall s \in S, t \in T \end{aligned} \tag{8}$$

where $P_{s,t}^{PV}$ and $P_{s,t}^{L}$ denote the scenario-dependent aggregated PV generation and residential demand, respectively, with $P_{s,t}^{L} = \sum_{h \in H} P_{h,s,t}^{L}$ (Equation (2)); $P_{s,t}^{grid}$ represents grid import; $P_{s,t}^{ESS,ch}$ and $P_{s,t}^{ESS,dis}$ are the shared-ESS charging and discharging powers; $P_{h,s,t}^{EV,ch}$ and $P_{h,s,t}^{EV,dis}$ denote the charging and V2H discharging powers, respectively, of the EV associated with household h; and $P_{s,t}^{curt}$ denotes curtailed PV power.

Grid export is not considered; therefore, grid power is restricted to a non-negative import. PV energy that cannot be directly consumed or stored is represented by the curtailment variable, which cannot exceed the available PV power:

$$P_{s,t}^{grid} \geq 0,\ 0 \leq P_{s,t}^{curt} \leq P_{s,t}^{PV},\ \forall s \in S, t \in T \tag{9}$$

Export is used only in the sensitivity analysis of Section 4.5: an exported power $P_{s,t}^{exp} \geq 0$ is added to the right-hand side of Equation (8) and remunerated at $\kappa\lambda_t$, so that $C_s = \sum_t \lambda_t \left(P_{s,t}^{\text{grid}} - \kappa P_{s,t}^{\text{exp}} \right) \Delta t$, and the grid import is limited by $P_{s,t}^{\text{grid}} \leq P_{max}^{\text{grid}}$, where P_{max}^{grid} is the grid-import limit, set in Section 4.5 as a percentage of the unconstrained peak import; in the main model, $\kappa = 0$ (no export) and the import is not limited.

3.4. Shared-ESS Operational Constraints

The shared ESS is subject to charging/discharging power limits, SOC dynamics, operating bounds, and mutually exclusive charging and discharging states. The charging and discharging powers are constrained by

$$0 \le P_{s,t}^{ESS,ch} \le P_{\max}^{ESS}\, u_{s,t}^{ESS,ch},\ 0 \le P_{s,t}^{ESS,dis} \le P_{\max}^{ESS} u_{s,t}^{ESS,dis},\ \forall s \in S, t \in T \tag{10}$$

where $P_{\max}^{ESS}$ is the rated power of the shared ESS, while $u_{s,t}^{ESS,ch}$ and $u_{s,t}^{ESS,dis}$ are binary variables indicating the charging and discharging states, respectively. Simultaneous charging and discharging are prevented by

$$u_{s,t}^{ESS,ch} + u_{s,t}^{ESS,dis} \le 1,\ \forall s \in S, t \in T \tag{11}$$

The ESS stored energy evolves according to

$$E_{s,t}^{ESS} = E_{s,t-1}^{ESS} + \eta_{ch}^{ESS} P_{s,t}^{ESS,ch} \Delta t - \frac{P_{s,t}^{ESS,dis} \Delta t}{\eta_{dis}^{ESS}},\ \forall s \in S, t \in T \tag{12}$$

where η_{ch}^{ESS} and η_{dis}^{ESS} denote the charging and discharging efficiencies, respectively. The stored energy is maintained within the allowable SOC range:

$$SOC_{min}^{ESS} E_{max}^{ESS} \le E_{s,t}^{ESS} \le SOC_{max}^{ESS} E_{max}^{ESS},\ \forall s \in S, t \in T \tag{13}$$

where E_{max}^{ESS} is the shared-ESS capacity and SOC_{min}^{ESS} and SOC_{max}^{ESS} are its minimum and maximum SOC limits. To ensure an energy-neutral daily scheduling cycle, the initial and terminal stored energies are specified as

$$E_{s,0}^{ESS} = SOC_{init}^{ESS} E_{max}^{ESS},\ E_{s,24}^{ESS} = SOC_{final}^{ESS} E_{max}^{ESS},\ \forall s \in S \tag{14}$$

In this study, both the initial and final ESS SOCs are set to 50%, thereby preventing the optimizer from exploiting the initially stored energy as free energy and enabling consistent comparison of ESS utilization among the investigated strategies. In the adaptive family, Equations (10) and (11) and the terminal condition of Equation (14) are replaced as described in Section 3.9.

3.5. EV Operational Constraints

Each household has one EV that can participate in community energy management through controlled charging and V2H discharging. The charging and discharging powers of each EV are constrained by

$$0 \le P_{h,s,t}^{EV,ch} \le P_{h,max}^{EV,ch} u_{h,s,t}^{EV,ch},$$

$$0 \le P_{h,s,t}^{EV,dis} \le P_{h,max}^{EV,dis} u_{h,s,t}^{EV,dis},\ \forall h \in H,\ s \in S,\ t \in T \tag{15}$$

where $P_{h,max}^{EV,ch}$ and $P_{h,max}^{EV,dis}$ are the maximum charging and discharging powers of the EV associated with household h, while $u_{h,s,t}^{EV,ch}$ and $u_{h,s,t}^{EV,dis}$ are the corresponding binary operating-state variables. Simultaneous charging and discharging are prevented by

$$u_{h,s,t}^{EV,ch} + u_{h,s,t}^{EV,dis} \le 1,\ \forall h \in H,\ s \in S,\ t \in T \tag{16}$$

In the implementation, a single binary per interval is used, with $u_{s,t}^{\mathrm{ESS,dis}} = 1 - u_{s,t}^{\mathrm{ESS,ch}}$, $u_{h,s,t}^{\mathrm{EV,dis}} = 1 - u_{h,s,t}^{\mathrm{EV,ch}}$, and this does not change the set of feasible power flows.

EV charging and V2H discharging are permitted only when the corresponding vehicle is connected to the household. Defining $a_{h,t}^{EV}$ as the EV availability parameter, the connection constraint is expressed as

$$u_{h,s,t}^{EV,ch} \le a_{h,t}^{EV},\ u_{h,s,t}^{EV,dis} \le a_{h,t}^{EV},\ \forall h \in H,\ s \in S,\ t \in T \tag{17}$$

EV h arrives at the clock hour t_h^{arr} and departs at t_h^{dep}, so that it is connected during the ordered intervals $T_h^{con} = \{t_h^{arr} + 1, \ldots, 24, 1, \ldots, t_h^{dep}\}$ (indices modulo 24), with $a_{h,t}^{EV} = 1$ for $t \in T_h^{con}$ and 0 otherwise. All EVs in Table 3 are connected across midnight.

During the connected period, the stored energy of EV h evolves according to its charging and V2H discharging activities:

$$E_{h,s,t}^{EV} = E_{h,s,\pi_h(t)}^{EV} + \eta_{h,ch}^{EV} P_{h,s,t}^{EV,ch} \Delta t - \frac{P_{h,s,t}^{EV,dis} \Delta t}{\eta_{h,dis}^{EV}}, \ \forall h \in H, \ s \in S, \ t \in T_h^{con} \tag{18}$$

where $E_{h,s,t}^{EV}$ is the energy stored at the end of interval t and $\pi_h(t)$ denotes the interval preceding t in the ordered set T_h^{con}. Hence $\pi_h(t_h^{arr} + 1) = t_h^{arr}$, whose energy is the arrival energy of Equation (21), and $\pi_h(1) = 24$ for connections spanning midnight. Since Equation (17) allows EV power only in T_h^{con} and Equation (18) holds for every interval of T_h^{con}, including the first one, every permitted charging and V2H discharging flow enters the energy balance; no energy enters or leaves the EV at the arrival instant t_h^{arr}, which is not an interval of T_h^{con}. The EV stored energy is maintained within its allowable SOC range ($\mathrm{SOC}_{\min} = 20\%$ and $\mathrm{SOC}_{\max} = 100\%$ for all EVs).

$$SOC_{h,min}^{EV} E_{h,max}^{EV} \le E_{h,s,t}^{EV} \le SOC_{h,max}^{EV} E_{h,max}^{EV}, \ \forall h \in H, \ s \in S, \ t \in T_h^{con} \tag{19}$$

To satisfy household mobility requirements, the EV SOC at its scheduled departure time (the end of the last connected interval) must meet the required departure SOC:

$$E_{h,s,t_h^{dep}}^{EV} \ge SOC_{h,dep}^{EV} E_{h,max}^{EV}, \ \forall h \in H, \ s \in S \tag{20}$$

Upon arrival, the stored energy of each EV is specified according to its corresponding arrival SOC:

$$E_{h,s,t_h^{arr}}^{EV} = SOC_{h,arr}^{EV} E_{h,max}^{EV}, \ \forall h \in H, \ s \in S \tag{21}$$

The EV parameters are given in Table 3. EV throughput is monitored for all strategies and limited in the proposed strategy (Equation (35)).

3.6. CVaR-Based Risk Formulation

To account for the financial risk arising from PV generation and residential demand uncertainties, the CVaR at confidence level α is incorporated using the Rockafellar–Uryasev formulation [37], in which the excess-cost variable is constrained by

$$z_s \ge C_s - \zeta, \ z_s \ge 0, \ \forall s \in S \tag{22}$$

where ζ is the VaR threshold and z_s represents the excess operating cost above ζ under scenario s. For N_s equiprobable scenarios, CVaR at confidence level α is calculated as

$$CVaR_\alpha = \zeta + \frac{1}{(1-\alpha)N_s} \sum_{s \in S} z_s \tag{23}$$

A confidence level of $\alpha = 0.90$ is adopted, so that $CVaR_{0.90}$ is the mean operating cost of the worst 10% of the scenarios. The risk-aware strategies restrict it through Equation (24).

$$CVaR_{0.90} \le \overline{(CVaR)} \tag{24}$$

where $\overline{(CVaR)}$ denotes the allowable upper bound on CVaR, determined in Section 3.8 ($\overline{R}_C$ of Equation (29) for the CVaR strategy and R_{AB} for the proposed strategy). When CVaR is not minimized, the auxiliary variables of Equations (22) and (23) need not take their smallest values and only bound the CVaR of the scenario costs from above; all reported CVaR values are therefore recomputed from the scenario costs as the mean of the $(1-\alpha)N_s$ largest costs (Section 4.1).

3.7. ESS Degradation Formulation

ESS cycling-related degradation is represented using the equivalent full cycle (EFC) metric as a throughput-based degradation proxy, which quantifies cumulative ESS energy throughput relative to twice its rated energy capacity. The ESS EFC over the scheduling horizon is calculated as

$$EFC^{ESS} = \frac{1}{N_s}\sum_{s\in S}\left[\frac{1}{2E^{ESS}_{max}}\sum_{t\in T}\left(\eta^{ESS}_{ch}P^{ESS,ch}_{s,t} + \frac{P^{ESS,dis}_{s,t}}{\eta^{ESS}_{dis}}\right)\Delta t\right] \tag{25}$$

where the charging and discharging efficiencies convert the grid-side ESS power flows to the corresponding battery-side energy throughput. A lower EFC^{ESS} therefore indicates reduced ESS cycling over the scheduling horizon. In the adaptive family, it is the expected EFC over the scenarios. The EFC does not capture the dependence of aging on the depth of discharge, the SOC range, and the charging rate, whose influence is examined in Section 4.5.

$$EFC^{ESS} \le \overline{EFC}^{ESS} \tag{26}$$

where $\overline{EFC}^{ESS}$ denotes the allowable upper bound on shared-ESS EFC, determined in Section 3.8 ($\overline{F}_E$ of Equation (32) for the EFC strategy). The EFC formulation applies exclusively to the shared ESS; EV battery degradation is not included in the degradation metric or constraint but is valued post hoc, like that of the ESS, with wear prices per kWh of battery-side throughput (Section 4.3).

3.8. ε-Constraint Strategy Formulation

The investigated strategies are formulated using a common expected-cost minimization objective with different ε-constraint settings and belong to two families: the static family (Baseline, CVaR, EFC, and Proposed (static)) with a day-ahead ESS schedule, and the adaptive family (Adaptive Baseline, Adaptive CVaR, Adaptive EFC, and Proposed (adaptive)) with the ESS dispatch of Section 3.9. Equations (27)–(33) define the static strategies; their adaptive counterparts solve the same problems with the adaptive dispatch and with all reference values taken from the Adaptive Baseline. The baseline strategy, which extends the model of [5] to the stochastic scenario set, minimizes the expected operating cost without additional CVaR or ESS-EFC constraints. The CVaR and EFC strategies impose individual upper bounds on operational risk and shared-ESS cycling, respectively, whereas the proposed strategy minimizes shared-ESS cycling within a cost budget, without increasing the CVaR (on the training scenarios) or the EV throughput of the Adaptive Baseline.

For the baseline strategy,

$$C_B = min\overline{C} \tag{27}$$

where C_B denotes the optimal expected operating cost of the baseline solution.

A risk-reference solution is obtained by minimizing CVaR subject to an allowable expected-cost tolerance:

$$\min CVaR_{0.90}, \text{s.t.}\overline{C} \le (1+\varepsilon_R)C_B \tag{28}$$

where ε_R denotes the economic tolerance used to construct the risk reference. If R_B and R_A denote the baseline and reference CVaR values, respectively, the CVaR bound for the risk-aware strategy is defined as

$$\overline{R}_C = R_B - \gamma_R(R_B - R_A),\ 0 < \gamma_R \le 1 \tag{29}$$

where γ_R specifies the fraction of the attainable CVaR reduction retained by the CVaR strategy.

The CVaR strategy is therefore formulated as

$$\min\overline{C},\ \text{s.t. } CVaR_{0.90} \le \overline{R}_C \tag{30}$$

Similarly, an ESS-cycling reference solution is obtained by minimizing shared-ESS EFC subject to an allowable expected-cost tolerance:

$$\min EFC^{ESS},\ \text{s.t.}\ \overline{C} \le (1+\varepsilon_D)C_B \tag{31}$$

where ε_D denotes the corresponding economic tolerance. Let F_B and F_A represent the baseline and reference ESS-EFC values, respectively. The EFC bound is defined as

$$\overline{F}_E = F_B - \gamma_D(F_B - F_A),\ 0 < \gamma_D \le 1 \tag{32}$$

where γ_D specifies the fraction of the attainable ESS-EFC reduction retained by the EFC strategy.

The EFC strategy is then formulated as

$$\min \overline{C}\ ,\ \text{s.t.}\ EFC^{ESS} \le \overline{F}_E \tag{33}$$

Both strategies are always feasible because the reference solutions satisfy the bounds. The values of ε_R, ε_D, γ_R, γ_D and the resulting bounds are reported in Section 4.2. The parameters ε_R, ε_D, γ_R, and γ_D define only the bounds of the CVaR and EFC strategies; the proposed strategy of Equation (35) does not use them, because its constraints are set by the Adaptive Baseline and by θ. Its sensitivity is therefore examined through θ (Section 4.3) and, for the alternative formulation with an EFC cap, through γ_D (Section 4.5).

The proposed strategy uses the adaptive dispatch and takes the expected cost C_{AB}, the CVaR R_{AB}, and the EV throughput Q_{AB} of the Adaptive Baseline as references, where the EV throughput is

$$Q^{EV} = \frac{1}{N_s}\sum_{s\in S}\sum_{h\in H}\sum_{t\in T_h^{\text{con}}}\left(\eta_{h,ch}^{EV}P_{h,s,t}^{EV,ch} + \frac{P_{h,s,t}^{EV,dis}}{\eta_{h,dis}^{EV}}\right)\Delta t \tag{34}$$

The proposed strategy minimizes the ESS EFC within a cost budget θ:

$$\min\ EFC^{ESS},\quad \text{s.t.}\ \overline{C} \le (1+\theta)C_{AB},\ CVaR_{0.90} \le R_{AB},\ Q^{\text{EV}} \le Q_{AB} \tag{35}$$

where $\theta = 1\%$ in the main case and 2% in the EFC-focused case. The Adaptive Baseline satisfies all constraints of Equation (35), so the problem is always feasible and requires no feasibility search. The proposed (static) strategy solves Equation (35) with the static dispatch and with C_B, R_B, and Q_B of the static Baseline in place of C_{AB}, R_{AB}, and Q_{AB}.

Remaining ties are resolved lexicographically, keeping each earlier optimum as a constraint: ESS EFC, expected cost, EV throughput, CVaR for proposed; expected cost, ESS EFC, EV throughput, CVaR for Baseline and CVaR; expected cost, CVaR, EV throughput for EFC.

3.9. Adaptive ESS Dispatch

In the adaptive family, the ESS is dispatched by a causal affine rule [38] that reacts to the deviation of the community net load from its nominal profile,

$$d_{s,t} = \left(P_{s,t}^{L} - P_{s,t}^{PV}\right) - \left(P_t^{L,0} - P_t^{PV,0}\right) \tag{36}$$

where $P_t^{L,0} = \sum_{h\in H} P_{h,t}^{L,0}$ and $P_t^{PV,0}$ are the nominal aggregated demand and PV generation of Section 2.5. The net ESS power, positive for charging, is

$$P_{s,t}^{ESS,ch} - P_{s,t}^{ESS,dis} = b_t + \sum_{l=1}^{M} K_{t,l}\, d_{s,t-l},\quad \forall s \in S,\ t \in T \tag{37}$$

with $M = 3$ preceding intervals (terms with $t - l < 1$ are omitted). The intercepts b_t and the gains $K_{t,l}$ are first-stage variables, identical in all scenarios; since $d_{s,t-l}$ is observed before

interval t, the rule is causal, and $K_{t,l} = 0$ recovers a static schedule. The ESS powers are continuous and bounded by

$$P^{ESS,ch}_{s,t} + P^{ESS,dis}_{s,t} \leq P^{ESS}_{max}, \quad P^{ESS,ch}_{s,t} \geq 0, \; P^{ESS,dis}_{s,t} \geq 0, \quad \forall s \in S, \; t \in T \tag{38}$$

in place of Equations (10) and (11). Equations (12) and (13) and the initial energy of Equation (14) hold in every scenario, and the terminal energy is

$$E^{ESS}_{s,24} \geq SOC^{ESS}_{final} E^{ESS}_{max}, \quad \forall s \in S \tag{39}$$

Equation (39) is enforced only on the training scenarios. In the test scenarios, the mean final ESS energy of the adaptive strategies is 49.96–50.04 kWh (target 50 kWh).

The other constraints of Sections 3.3–3.6 are the same as in the static family, and the binary variables belong only to the EVs. The parameters b_t and $K_{t,l}$ are designed offline on the training scenarios together with the EV schedule and executed online: in each interval, the set-point of Equation (37) is computed from the measured deviations and limited by the power rating, the SOC window, and the community demand (no export). Its positive and negative parts represent charging and discharging power, so simultaneous charging and discharging do not occur.

3.10. Optimization Procedure

The overall optimization procedure is illustrated in Figure 3. The input data and system parameters are first initialized, followed by generation of stochastic PV and load scenarios. The baseline solution is then obtained, and the risk and ESS-cycling reference solutions are determined to establish the corresponding ε-constraint bounds. The CVaR and EFC strategies are subsequently solved using their individual bounds. The procedure is repeated for the adaptive family with the dispatch of Section 3.9, where the proposed strategy is solved with the cost budget, CVaR, and EV throughput of the Adaptive Baseline. All strategies are evaluated on the same independent test scenarios (Section 4.2).

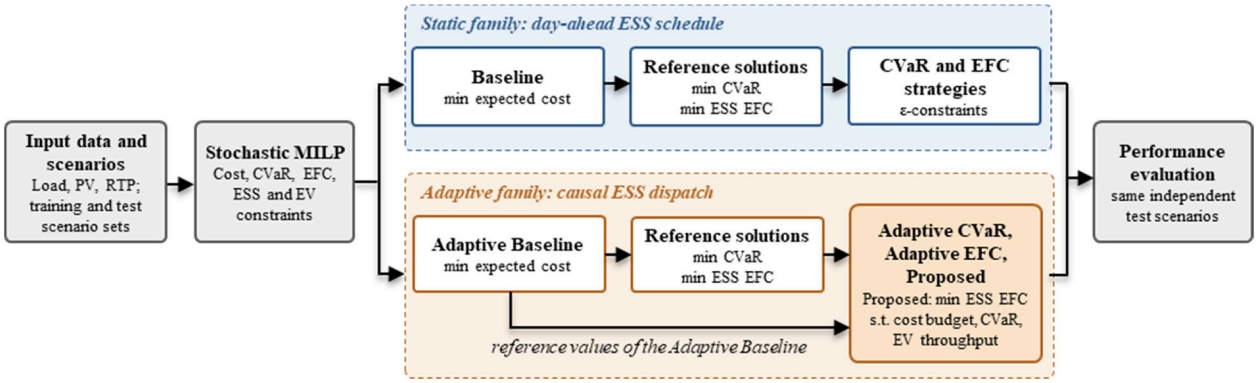


Figure 3. Flowchart of the stochastic MILP optimization procedure for the investigated strategies.

4. Results and Discussion

4.1. Benchmark Reproduction and Model Verification

Before evaluating the proposed stochastic framework, the deterministic three-home benchmark reported in [5] was reproduced to verify the numerical implementation of the underlying energy management model. The reproduction employed the same benchmark dataset, RTP tariff, PV and ESS specifications, EV parameters, appliance requirements, operating constraints, and currency unit, with operating costs reported in Danish kroner (DKK) to ensure direct comparability.

As shown in Table 4, the reproduced community operating cost is 288.25 DKK/day compared with the published value of 287.50 DKK/day, corresponding to an aggregate error of only 0.26%, while the largest household-level deviation is 2.40% for SH3. The close agreement supports the correctness of the deterministic cost-minimization and energy-balance implementation. The reproduced formulation is the Baseline of the static family and is extended with stochastic PV and load uncertainties, CVaR-based risk management, a causal-adaptive ESS recourse, and EFC-based mitigation of ESS cycling-related degradation.

Table 4. Comparison of published benchmark [5] and reproduced results for model verification.

Home	Published Benchmark [5] (DKK/Day)	Reproduced Result (DKK/Day)	Relative Error (%)
SH1	110.47	109.78	0.62
SH2	93.36	92.78	0.62
SH3	83.67	85.68	2.4
Total	287.5	288.25	0.26

DKK is Danish kroner.

The optimized schedules of all strategies (first training seed) were checked against the model constraints with the hourly indexing of Section 3.1. The EV energy-balance residual, EV flow outside the connection window, EV departure-SOC shortfall, EV SOC-bound violation, and simultaneous EV charging and discharging were all below 1×10^{-6} (kWh or kW), within the solver feasibility tolerance.

Table 5 compares the CVaR from the auxiliary variables of Equations (22) and (23) with the CVaR recomputed from the scenario costs for the first-stage solution of the first training seed. The two coincide for the CVaR-constrained strategies and differ by 19–22 DKK/day for the others (Section 3.6); all CVaR values in this paper are therefore recomputed from the final scenario-cost distribution. The recomputed Baseline values (604.1 and 590.8) are slightly above the references of Table 6 (603.79 and 590.63), which are obtained after the final CVaR stage.

Table 5. CVaR of the solution of the first lexicographic stage: auxiliary variables versus recomputation from the scenario costs (first training seed, DKK/day).

Strategy	Auxiliary Variables	Recomputed from Scenario Costs	Difference
Baseline (static)	626.0	604.1	21.9
CVaR (static)	595.3	595.3	0.0
EFC (static)	635.0	613.2	21.8
Baseline (adaptive)	610.0	590.8	19.2
Proposed (adaptive)	590.6	590.6	0.0

4.2. Evaluation Protocol and Parameters

The static family (Baseline, CVaR, EFC, and Proposed (static)) and the adaptive family (Adaptive Baseline, Adaptive CVaR, Adaptive EFC, and Proposed (adaptive)) are defined in Section 3.8; Proposed (adaptive) is the proposed (CVaR+EFC) strategy, referred to as proposed in the text, with $\theta = 1\%$ as the main case and $\theta = 2\%$ as the EFC-focused case. Results are reported against the static Baseline (total improvement over [5]) and the Adaptive Baseline (effect of the constraints alone).

Table 6. Reference values and anchors per training seed.

Family	Quantity	Seed 42	Seed 1042	Seed 2042
Static	Baseline: expected cost C_B (DKK/day)	536.26	530.03	534.23
	Baseline: CVaR R_B (DKK/day)	603.79	603.42	616.71
	Baseline: ESS EFC F_B (cycles/day)	0.6000	0.6000	0.6000
	Baseline: EV throughput Q_B (kWh/day)	168.87	174.74	166.22
	Risk reference R_A (DKK/day)	594.36	595.00	606.93
	EFC reference F_A (cycles/day)	0.5493	0.5499	0.5495
	CVaR cap R_C (DKK/day)	595.30	595.84	607.91
	EFC cap F_E (cycles/day)	0.5569	0.5574	0.5571
Adaptive	Adaptive Baseline: expected cost (DKK/day)	529.94	522.99	524.52
	Adaptive Baseline: CVaR (DKK/day)	590.63	585.23	599.84
	Adaptive Baseline: ESS EFC (cycles/day)	0.6000	0.6000	0.6000
	Adaptive Baseline: EV throughput (kWh/day)	162.93	166.66	166.77
	Adaptive risk reference (DKK/day)	579.89	578.11	588.74
	Adaptive EFC reference (cycles/day)	0.5476	0.5473	0.5472
	Adaptive CVaR cap (DKK/day)	580.97	578.82	589.85
	Adaptive EFC cap (cycles/day)	0.5554	0.5552	0.5551
Settings	Cost tolerance of the risk reference, ε_R	0.015	0.015	0.015
	Cost tolerance of the EFC reference, ε_D	0.02	0.02	0.02
	Risk share γ_R	0.9	0.9	0.9
	EFC share γ_D	0.85	0.85	0.85

Table 6 lists, for each training seed, the reference solutions, the CVaR and EFC bounds of Equations (29) and (32), and the settings ε_R, ε_D, γ_R, and γ_D. Each strategy is trained on three sets of 100 scenarios (seeds 42, 1042, 2042) and tested on the five independent test sets of Section 2.5; results are means over the training seeds, each averaged over the test sets. The main results (Tables 7–9, Figures 4–7) use the five test sets of 5000 scenarios; the sensitivity analyses (Tables 10–12, Figure 8a) use two test sets of 2000 scenarios (seeds 10,001 and 10,002), and Figure 8b uses the training scenarios.

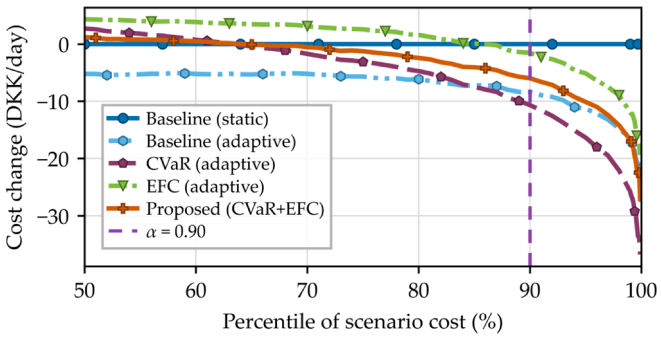


Figure 4. Out-of-sample scenario-cost distributions of the investigated strategies: differences in the scenario-cost percentiles relative to the static Baseline (first training seed).

4.3. Cost, Risk, and ESS Degradation Trade-Off

Table 7 gives the out-of-sample performance of all strategies, and Table 8 the changes relative to a stated reference: Block A (static strategies vs. the static Baseline), Block B (adaptive strategies vs. the Adaptive Baseline, i.e., the effect of the constraints alone), and Block C (adaptive strategies vs. the static Baseline, i.e., the total improvement over [5]). Relative to the static benchmark, the proposed (CVaR+EFC) strategy with $\theta = 1\%$ lowers expected cost by 0.24%, CVaR by 2.18%, and ESS cycling by 4.37%, with the same sign in

every training seed; relative to the Adaptive Baseline, it trades a 1.12% cost increase for a 4.46% reduction in ESS cycling at a practically unchanged CVaR (+0.16%).

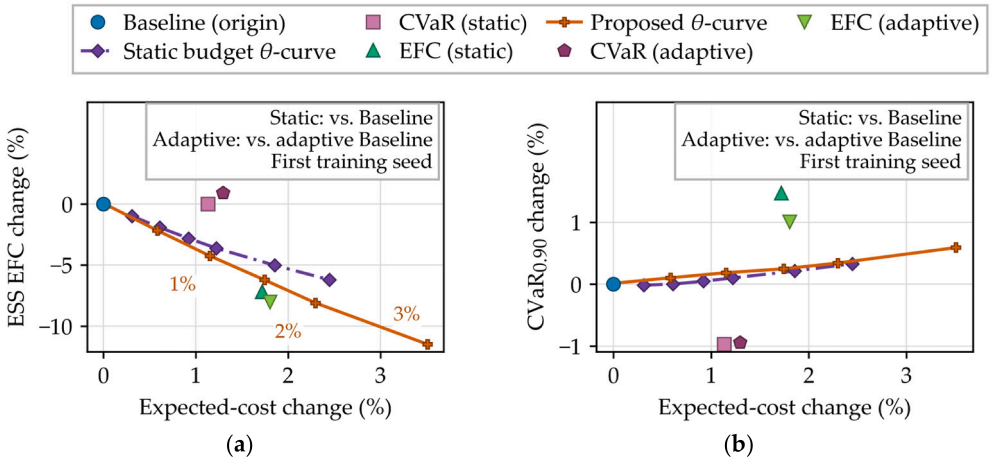


Figure 5. Cost-risk-ESS degradation trade-offs among the investigated strategies (first training seed): (**a**) cost–EFC trade-off, and (**b**) cost–CVaR trade-off.

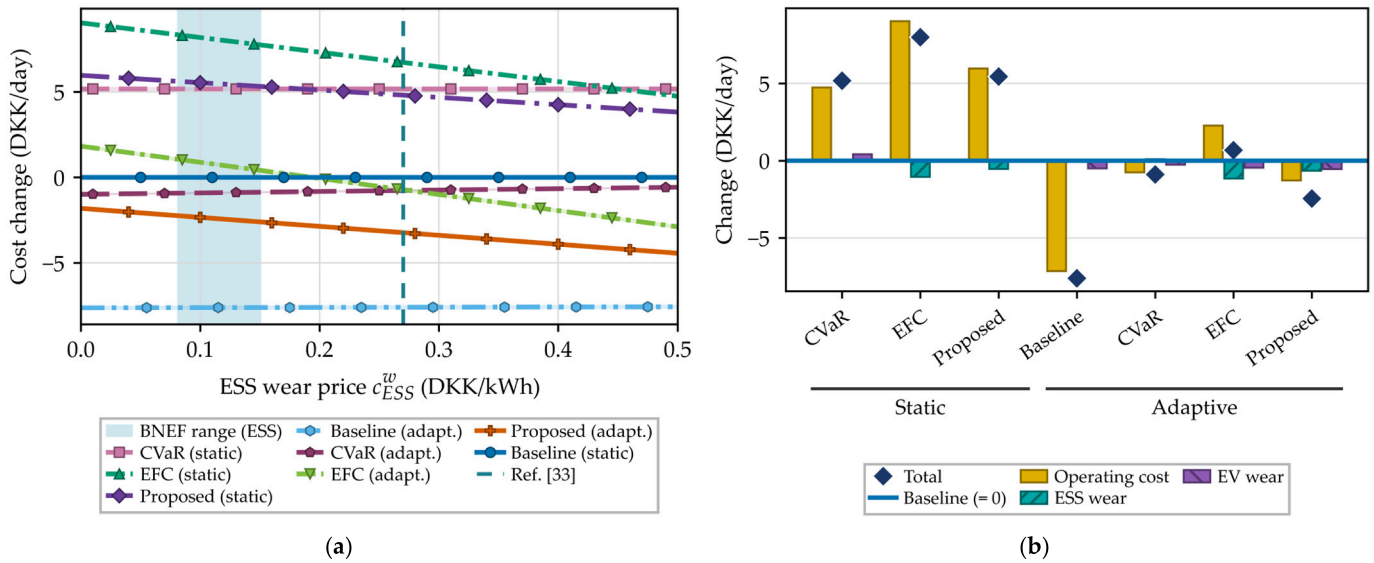


Figure 6. Degradation-inclusive daily cost relative to the static Baseline: (**a**) total cost versus the ESS wear price (EV wear price 0.08–0.14 DKK/kWh) and (**b**) cost components at the BNEF reference basis.

Table 7 lists the absolute results. The EV throughput of the proposed strategy (165.04 kWh/day for θ = 1%) does not exceed that of the Adaptive Baseline (165.45 kWh/day), as required by Equation (35), so its lower ESS cycling is not obtained by shifting cycling to the EV batteries; the reduction relative to the static Baseline (−2.85%, Table 8) is not seed-robust, and this is not claimed. The no-export violation is the share of test scenarios in which the scheduled ESS discharge exceeds the community demand for at least one hour even with all PV curtailed; the grid import is then zero, and the cost is unaffected, so these scenarios are retained. The share is 2.8–3.4% for the static strategies and at most 0.10% for the adaptive ones, because the ESS absorbs PV forecast errors that a day-ahead schedule cannot.

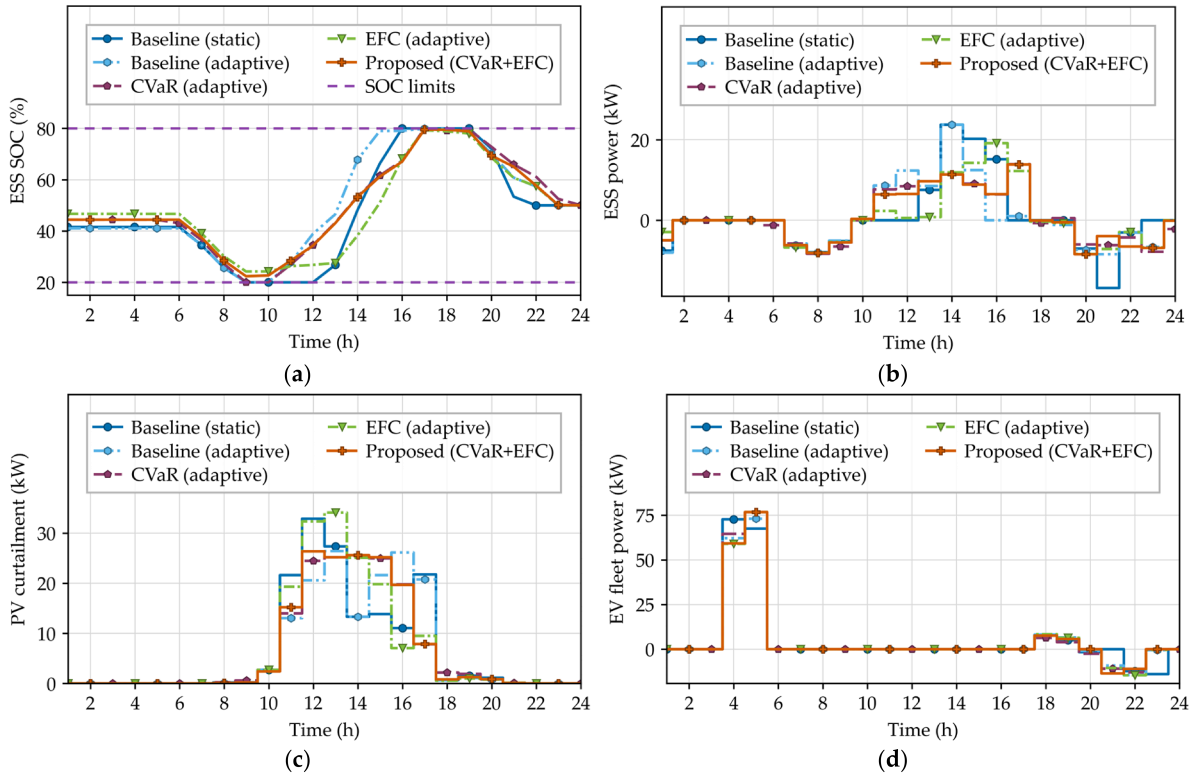


Figure 7. Hourly operation of the investigated strategies for the ten-home community (first training seed, first test set): (**a**) shared-ESS SOC, (**b**) shared-ESS power, (**c**) PV curtailment, and (**d**) aggregated EV power.

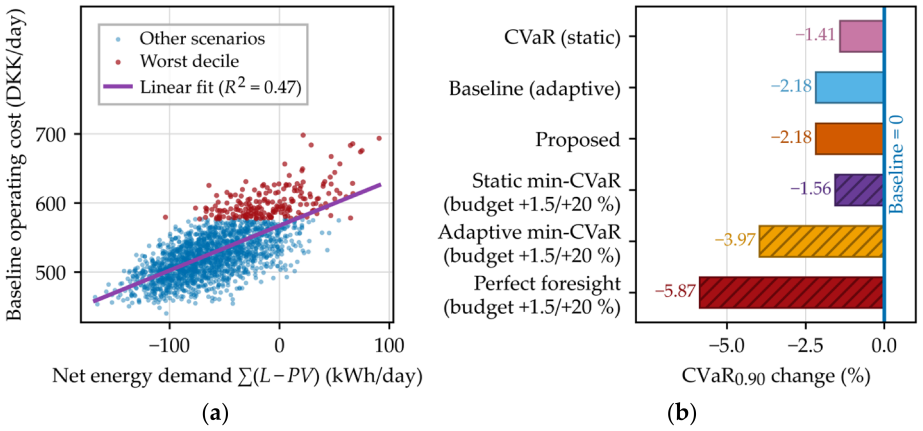


Figure 8. Cost drivers and CVaR-reduction limit: (**a**) net demand versus Baseline cost (first 2000-scenario test set), and (**b**) CVaR change relative to the static Baseline on the training scenarios of the first training seed (in-sample).

Table 7. Out-of-sample performance of all strategies (mean over 3 training seeds × 5 test sets of 5000 scenarios).

Method	Expected Cost (DKK/Day)	CVaR$_{0.90}$ (DKK/Day)	ESS EFC (Cycles/Day)	EV Throughput (kWh/Day)	No-Export Violations (%)	Total incl. Wear (DKK/Day)
Baseline (static)	529.00	605.51	0.600	169.94	2.78	557.58–566.93
CVaR (static)	533.75	599.30	0.600	173.83	3.40	562.65–572.21
EFC (static)	538.04	614.36	0.557	169.95	2.78	565.57–574.92
Proposed (static), θ = 1%	534.97	605.98	0.579	169.94	2.81	563.02–572.37

Table 7. *Cont.*

Method	Expected Cost (DKK/Day)	$CVaR_{0.90}$ (DKK/Day)	ESS EFC (Cycles/Day)	EV Throughput (kWh/Day)	No-Export Violations (%)	Total incl. Wear (DKK/Day)
Proposed (static), θ = 2%	540.81	606.99	0.563	169.94	3.17	568.48–577.83
Baseline (adaptive)	521.87	591.39	0.601	165.45	0.10	550.09–559.19
CVaR (adaptive)	528.26	586.33	0.604	167.70	0.00	556.75–565.97
EFC (adaptive)	531.28	595.84	0.553	165.84	0.06	558.37–567.49
Proposed (adaptive), θ = 1%	527.73	592.32	0.574	165.04	0.03	555.26–564.34
Proposed (adaptive), θ = 2%	533.52	593.14	0.551	165.45	0.01	560.52–569.62

Note: Total incl. wear: EV wear price 0.082–0.137 DKK/kWh, ESS wear price 0.122 DKK/kWh (Section 4.3).

Table 8. Change relative to the stated reference (mean, with the range over training seeds in brackets).

Method	Δ Cost (%)	Δ CVaR (%)	Δ ESS EFC (%)	Δ EV thr. (%)	Δ Total incl. Wear (DKK/Day)
A. Static methods: change relative to the static Baseline					
CVaR (static)	+0.90 [+0.67, +1.13]	−1.02 [−1.28, −0.81]	0.00 [0.00, 0.00]	+2.29 [+2.09, +2.58]	+5.07 to +5.28
EFC (static)	+1.71 [+1.70, +1.72]	+1.46 [+1.44, +1.47]	−7.15 [−7.18, −7.10]	0.00 [0.00, +0.01]	+7.99
Proposed (static), θ = 1%	+1.13 [+1.04, +1.22]	+0.08 [+0.02, +0.12]	−3.58 [−3.63, −3.52]	0.00 [0.00, 0.00]	+5.44
Proposed (static), θ = 2%	+2.23 [+2.07, +2.45]	+0.25 [+0.04, +0.37]	−6.14 [−6.21, −6.10]	0.00 [0.00, 0.00]	+10.90
B. Adaptive methods: change relative to the Adaptive Baseline (effect of the CVaR and EFC constraints)					
CVaR (adapt.)	+1.22 [+1.11, +1.29]	−0.85 [−0.97, −0.65]	+0.59 [−0.18, +1.04]	+1.36 [+0.83, +1.64]	+6.66 to +6.78
EFC (adapt.)	+1.80 [+1.78, +1.83]	+0.75 [+0.53, +1.00]	−7.94 [−8.03, −7.79]	+0.23 [+0.07, +0.48]	+8.28 to +8.30
Proposed (adapt.), θ = 1%	+1.12 [+1.10, +1.15]	+0.16 [+0.06, +0.23]	−4.46 [−4.74, −4.25]	−0.25 [−0.75, 0.00]	+5.15 to +5.17
Proposed (adapt.), θ = 2%	+2.23 [+2.17, +2.30]	+0.29 [+0.13, +0.41]	−8.30 [−8.75, −8.05]	0.00 [0.00, 0.00]	+10.43
C. Adaptive methods: change relative to the static Baseline (benchmark derived from Ref. [5])					
Baseline (adapt.)	−1.35 [−1.67, −1.17]	−2.33 [−2.52, −2.02]	+0.10 [−0.04, +0.18]	−2.60 [−4.63, +0.33]	−7.73 to −7.49
CVaR (adapt.)	−0.14 [−0.42, +0.11]	−3.17 [−3.46, −2.94]	+0.69 [−0.02, +1.09]	−1.27 [−3.83, +1.97]	−0.95 to −0.83
EFC (adapt.)	+0.43 [+0.13, +0.61]	−1.60 [−1.94, −1.03]	−7.85 [−7.88, −7.82]	−2.38 [−4.48, +0.40]	+0.56 to +0.79
Proposed (adapt.), θ = 1%	−0.24 [−0.59, −0.04]	−2.18 [−2.40, −1.84]	−4.37 [−4.59, −4.07]	−2.85 [−4.63, +0.32]	−2.59 to −2.32
Proposed (adapt.), θ = 2%	+0.85 [+0.47, +1.10]	−2.04 [−2.33, −1.68]	−8.21 [−8.60, −7.94]	−2.61 [−4.63, +0.33]	+2.70 to +2.94

Note: θ: cost budget over the Baseline of the same dispatch rule. Total incl. wear: ESS wear price 0.122 DKK/kWh, EV wear price 0.082–0.137 DKK/kWh.

Table 9. PV utilization, curtailment, and grid import of the main strategies (first training seed, first test set of 5000 scenarios).

Quantity	Baseline (Static)	Baseline (Adaptive)	CVaR (Adaptive)	EFC (Adaptive)	Proposed (CVaR+EFC), θ = 1%
PV (kWh/day)	347.75	347.75	347.75	347.75	347.75
Curtailed (kWh/day)	148.39	147.59	150.44	152.74	150.99
PV utilization (%)	57.33	57.56	56.74	56.08	56.58
Grid import (kWh/day)	226.42	225.00	228.32	229.23	227.76
Import 01–06 h (%)	84.40	82.51	84.74	83.46	83.18
Import 07–17 h (%)	1.86	2.07	1.47	1.44	1.63
Import 18–24 h (%)	13.74	15.42	13.79	15.10	15.20
Curtailment, ESS full (%)	23.58	14.67	5.22	0.14	0.30
Curtailment, ESS at power limit (%)	0.00	0.21	0.04	0.10	0.04
Curtailment, ESS not saturated (%)	76.42	85.11	94.74	99.76	99.66
Curtailment hours with import in the same day (%)	100.00	100.00	100.00	100.00	100.00

Table 10. Sensitivity of the proposed strategy ($\theta = 1\%$) to design and operating parameters (training seed 42).

Case	Baseline Cost (DKK/Day)	Δ Cost (%)	Δ CVaR (%)	Δ EFC (%)	Δ Cost (%)	Δ CVaR (%)	Δ EFC (%)	PV Not Used Locally	
		vs. Static			vs. Adaptive			Baseline (%)	Proposed (%)
ESS SOC window									
SOC 20–80%	528.24	0.00	−1.78	−4.10	1.16	0.19	−4.27	42.68	43.42
SOC 10–90%	483.10	−0.12	−1.95	−3.13	1.15	0.08	−3.24	36.32	37.02
SOC 30–70%	573.81	0.05	−1.64	−6.62	1.14	0.13	−6.66	49.04	49.79
ESS power rating									
0.25C	528.24	0.00	−1.78	−4.10	1.16	0.19	−4.27	42.68	43.42
0.125C	528.09	0.02	−1.67	−4.43	1.15	0.21	−4.40	42.66	43.43
0.5C	528.17	0.01	−1.64	−4.18	1.12	0.08	−4.49	42.67	43.43
EFC threshold (Proposed with EFC cap)									
$\gamma_D = 0.25$	528.24	−0.57	−1.86	−2.03	0.59	0.10	−2.20	42.68	42.97
$\gamma_D = 0.5$	528.24	0.07	−1.77	−4.36	1.23	0.20	−4.53	42.68	43.48
$\gamma_D = 0.85$	528.24	1.03	−1.61	−7.62	2.20	0.36	−7.78	42.68	44.16
$\gamma_D = 1$	528.24	1.49	−1.48	−8.98	2.67	0.49	−9.15	42.68	44.47
PV size and export									
PV × 1, $\kappa = 0$	528.24	0.00	−1.78	−4.10	1.16	0.19	−4.27	42.68	43.42
PV × 0.5, $\kappa = 0$	615.95	−0.21	−1.42	−8.13	1.06	0.24	−8.13	6.18	7.66
PV × 1.5, $\kappa = 0$	475.58	−0.01	−1.89	−4.15	1.16	0.22	−4.11	57.68	58.09
PV × 2, $\kappa = 0$	434.86	0.03	−1.87	−3.72	1.12	0.16	−3.83	65.80	66.09
PV × 1, $\kappa = 0.5$	285.22	1.04	0.07	−5.36	1.18	0.16	−8.78	70.18	71.05
PV × 0.5, $\kappa = 0.5$	535.72	0.87	−0.17	−15.29	1.10	0.06	−21.59	51.36	55.12
PV × 1.5, $\kappa = 0.5$	53.17	0.86	−0.15	−0.99	1.52	0.03	−4.83	77.88	77.98
Import limit									
No limit	528.24	0.00	−1.78	−4.10	1.16	0.19	−4.27	42.68	43.42
80% of peak	528.63	0.00	−1.76	−4.14	1.17	0.19	−4.31	42.64	43.43
60% of peak	529.39	0.01	−1.73	−4.15	1.16	0.20	−4.33	42.63	43.42

Table 11. Sensitivity of the proposed strategy ($\theta = 1\%$) to the number of training scenarios and to the uncertainty scale.

Case	Baseline Cost (DKK/Day)	Δ Cost (%)	Δ CVaR (%)	Δ EFC (%)	Δ Cost (%)	Δ CVaR (%)	Δ EFC (%)	Training Seeds
		vs. Static			vs. Adaptive			
Training scenarios								
$N_s = 25$	527.29	−0.15	−2.09	−3.11	0.88	0.22	−3.63	3
$N_s = 50$	527.54	−0.07	−1.88	−3.99	1.05	0.37	−4.67	3
$N_s = 100$	528.68	−0.22	−2.11	−4.38	1.13	0.14	−4.48	3
$N_s = 200$	530.67	−0.38	−2.66	−4.33	1.03	−0.02	−4.35	3
$N_s = 400$	530.37	−0.45	−2.73	−3.96	0.99	−0.01	−3.97	3
Uncertainty scale								
$\sigma = 0.5$	513.59	0.67	−0.71	−3.77	1.14	0.19	−4.03	1
$\sigma = 1$	528.24	0.00	−1.78	−4.10	1.16	0.19	−4.27	1
$\sigma = 1.5$	543.96	−0.45	−2.03	−4.58	1.15	0.34	−4.72	1
$\sigma = 2$	559.60	−0.70	−2.57	−5.00	1.07	−0.02	−7.04	1

Table 12. Effect of the relative MIP gap tolerance on the 24 solves of the proposed strategy ($\theta = 1\%$) and its reference solutions (first training seed; two test sets of 2000 scenarios).

Quantity	10^{-6}	10^{-4}	10^{-3}	5×10^{-3}
Solves reported optimal	24 of 24	24 of 24	24 of 24	24 of 24
Proposed cost (DKK/day)	528.2	528.2	528.2	528.2
Proposed Δ cost (%)	−0.005	−0.005	−0.005	−0.005
Proposed CVaR (DKK/day)	589.6	589.6	589.6	589.6
Proposed Δ CVaR (%)	−1.78	−1.78	−1.78	−1.78
Proposed ESS EFC (cycles/day)	0.5754	0.5754	0.5754	0.5754
Proposed Δ ESS EFC (%)	−4.10	−4.10	−4.10	−4.10
Maximum achieved relative gap	$<10^{-9}$	$<10^{-9}$	$<10^{-9}$	$<10^{-9}$

Table 8 (Block A) shows that, among the static strategies, the CVaR cap lowers CVaR by 1.02% for a 0.90% cost increase without reducing ESS cycling and with 2.29% higher EV throughput; the EFC cap lowers cycling by 7.15% for a 1.71% cost increase but raises the CVaR by 1.46%. Proposed (static), i.e., the proposed strategy without the adaptive dispatch, lowers cycling by 3.58% ($\theta = 1\%$) and 6.14% ($\theta = 2\%$) for cost increases of 1.13% and 2.23%, with no change in EV throughput, but obtains no CVaR reduction (+0.08% and +0.25%).

Table 8 (Block B) isolates the effect of the constraints, because the Adaptive Baseline already contains the causal recourse. The CVaR cap lowers CVaR by 0.85% for a 1.22% cost increase without reducing ESS cycling (+0.59%, range including zero); the EFC cap lowers cycling by 7.94% for a 1.80% cost increase but raises CVaR by 0.75%. The proposed strategy (adapt.) avoids this conflict: with $\theta = 1\%$, cycling falls by 4.46% with CVaR within 0.16%, and with $\theta = 2\%$ by 8.30% for a 2.23% cost increase (3.7–4.0% less cycling per 1% of cost). Its CVaR is not lower than that of the Adaptive Baseline, so its CVaR advantage over the static Baseline comes from the adaptive recourse.

Table 8 (Block C) compares the adaptive strategies with the static Baseline: all of them lower CVaR (−1.60% to −3.17%). The proposed strategy (adapt.) with $\theta = 1\%$ simultaneously lowers the expected cost (−0.24%), CVaR (−2.18%), ESS cycling (−4.37%), and the wear-inclusive daily total (−2.59 to −2.32 DKK/day); with $\theta = 2\%$, cycling falls by 8.21% and CVaR by 2.04% at an expected cost 0.85% above the static Baseline.

Overfitting check. Averaged over the three training seeds, the CVaR on the training scenarios is 607.97, 591.90, and 599.68 DKK/day for the static Baseline, the Adaptive Baseline, and the static CVaR strategy, against 605.51, 591.39, and 599.30 DKK/day on the test scenarios (Table 7), i.e., within 0.5%, so the reductions in Table 8 are not an artifact of overfitting.

Figure 4 shows the differences between the scenario-cost percentiles of each strategy and those of the static Baseline. The adaptive CVaR, adaptive EFC, and proposed strategies have lower costs in the worst-decile scenarios (percentiles above 90), in line with Table 8; the adaptive EFC strategy has higher costs up to about the 85th percentile because its stronger cycling limit restricts the economic use of the ESS.

Figure 5 shows the change in ESS EFC (a) and in CVaR (b) against the change in expected cost, each family relative to its own Baseline. Along the proposed curve, the ESS EFC falls almost linearly with the added cost while the CVaR rises only slightly; the static budget curve (the same cost budget θ applied to the static family, with the CVaR and EV throughput of the static Baseline as bounds) gives a smaller cycling reduction and no CVaR reduction. The CVaR strategies lower CVaR, but not cycling, and the EFC strategies do the opposite.

The total including wear is

$$C^{tot} = \overline{C} + c^{w}_{ESS} Q^{ESS} + c^{w}_{EV} Q^{EV}, \quad Q^{ESS} = 2E^{ESS}_{max}\, EFC^{ESS} \tag{40}$$

with $c^{w}_{\mathrm{ESS}} = 0.122$ DKK/kWh and $c^{w}_{\mathrm{EV}} = 0.082$–$0.137$ DKK/kWh; the two values in each cell correspond to the lower and upper EV wear price.

Wear prices. Degradation is valued post hoc with wear prices c^{w}_{ESS} and c^{w}_{EV} (DKK per kWh of battery-side throughput), given by

$$c^{w} = \frac{(1 - \text{residual} - \text{value share}) \times (\text{battery price} \times \text{exchange rate})}{2 \times \text{cycle life} \times \text{DoD}} \tag{41}$$

where c^{w} denotes c^{w}_{ESS} or c^{w}_{EV}, with DoD = 80% and an exchange rate of 6.62 DKK/USD (2025 average). For the ESS, the base case uses the BloombergNEF (BNEF) turnkey stationary-storage price for Europe in 2025, 177 USD/kWh [39], and 6000 cycles, within the ranges reported for grid-scale lithium-ion systems [40] and above the 2640 cycles assumed for 2030 LFP in [41], giving 0.122 DKK/kWh. Varying one parameter at a time gives 0.081–0.151 DKK/kWh for the global average price of 117 USD/kWh and the US price of 219 USD/kWh [39], and 0.183 and 0.092 DKK/kWh for 4000 and 8000 cycles; 0.27 DKK/kWh, derived from the levelized cost of storage of 0.072 EUR/kWh in [33] (7.46 DKK/EUR, halved per kWh of battery-side throughput), is used as an upper bound. For the EV pack, the BNEF battery-pack price for battery electric vehicles of 99 USD/kWh [42], an assumed 3000 cycles, and an assumed residual value of 40% give 0.082 DKK/kWh (0.137, 0.273, and 0.051 DKK/kWh without residual value for 3000, 1500, and 8000 cycles). Since the EV cycle life and residual value are assumptions, wear-inclusive results are reported as ranges.

Figure 6 shows the daily total including wear relative to the static Baseline for ESS wear prices from 0 to 0.5 DKK/kWh (a) and its cost components at the BNEF reference basis (b). The proposed strategy with $\theta = 1\%$ is cheaper than the static Baseline in every seed (operating cost −1.28, ESS wear −0.64, and EV wear −0.54 DKK/day at the base ESS price and mid-range EV price), but about 5.2 DKK/day more expensive than the Adaptive Baseline, because its 4.46% lower ESS throughput (about 5.4 kWh/day) is worth less than the 5.9 DKK/day of additional operating cost. Extrapolating beyond Figure 6a, the two would break even at about 1.1 DKK/kWh, six to fourteen times the ESS wear prices used and four times the upper value of [33]. At present battery prices, the strategy is therefore a controllable means of reducing ESS cycling at a known, small price, relevant when degradation costs exceed the assumed values, when warranty or cycle-count limits apply, or when the ESS serves other purposes.

4.4. Operating Mechanism, PV Curtailment, and CVaR-Reduction Limit

Figure 7 shows the 24 h operation of the ten-home community. In all strategies, EV charging is concentrated in the low-tariff hours (Figure 2c), the shared-ESS charges from PV between about 10 and 17 h and discharges in the evening, and the SOC returns to its terminal target. The proposed strategy spreads the midday ESS charging over a longer window with a maximum of about 14 kW, against peaks of 20–24 kW for the static and Adaptive Baselines, and reaches the 80% SOC limit at 16–19 h; this lower charging peak is the visible form of its 4.46% lower ESS throughput (Table 8), and the curtailed PV is correspondingly flatter (a plateau of about 25 kW instead of peaks of 33–34 kW).

Table 9 shows where the effect of the lower cycling appears (first training seed and first test set; PV utilization is the share of the available PV energy that is not curtailed). Relative to the Adaptive Baseline, the proposed strategy curtails 3.4 kWh/day more PV (+2.3%; utilization 57.6% to 56.6%) and imports 2.8 kWh/day more (+1.2%), which is the physical origin of its 1.12% higher operating cost. Relative to the static Baseline, curtailment and import are 2.6 and 1.3 kWh/day higher, more than offset by the lower prices obtained with adaptive dispatch (Table 8, Block C).

Curtailment mechanism. Curtailment occurs at midday (about 10–17 h, Figure 7), whereas 82–85% of the import occurs between 01 and 06 h in all strategies (Table 9). About 43% of the PV energy (148 kWh/day) is curtailed as a result of the no-export model, in which PV energy that can be neither consumed nor stored is curtailed; the effect of export is examined in Section 4.5. Curtailment is set mainly by the daily energy capacity of the ESS: its usable window (20–80% of 100 kWh) is 60 kWh, much smaller than the curtailed energy, and the community still imports energy on the same day in all curtailment hours (Table 9). The strategies without an EFC reduction operate at 0.600 cycles/day, i.e., one full swing of this window per day (about 120 kWh of charge plus discharge), a result of the optimization and not a model constraint; the proposed strategy, at 0.574, swings it about 4% less, consistent with its 3.4 kWh/day of additional curtailed PV. The classification of Table 9 (ESS full, at its power limit, or not saturated) is a snapshot at the curtailment hour; since the ESS reaches its upper SOC limit later in the afternoon (Figure 7a), a "not saturated" hour does not indicate spare capacity.

ESS–EV coupling. The EV schedule is fixed a day ahead and is identical in all scenarios, whereas the ESS dispatch adapts to the realized scenario. The two are therefore coupled only through the shared grid import and the PV surplus, not through a common state. EV and ESS charging both draw on the same night-time import (Table 9). Since EVs are away during the PV peak (Section 2.4), reducing ESS cycling in the proposed strategy appears directly as additional curtailment (Table 9) and is not offset by EV charging. The grid connection is not a binding coupling: limiting the import to 60% of its unconstrained peak leaves the indicators practically unchanged (Section 4.5, Table 10).

CVaR-reduction limit. The CVaR reductions in Table 8 are modest because little of the tail risk is controllable by the ESS. Figure 8a shows, for the 2000 scenarios of the first test set (first training seed), that the daily net energy demand (load minus PV) explains 47% of the variance of the Baseline operating cost, and that the worst decile of costs consists of days with little PV surplus (mean net demand −7.0 kWh/day against −65.5 kWh/day in the other scenarios). The proposed strategy lowers the cost of these scenarios by 11.8 DKK/day on average relative to the static Baseline and raises the cost of the others by 1.05 DKK/day, which is how CVaR falls at an almost unchanged expected cost. Figure 8b shows the largest CVaR reduction that any ESS policy can reach for the training scenarios of the first seed within a cost increase of 1.5%: −1.56% for a static schedule, −3.97% for a causal-adaptive policy, and −5.87% for perfect foresight, with the same values for a 20% budget, so the limit is not set by the cost budget. The static CVaR strategy (−1.41%) reaches about 90% of the static limit, in line with the risk share of 0.9, and the Adaptive Baseline and the proposed strategy (−2.18%) lie between the static and the causal-adaptive limit. Even perfect foresight reduces CVaR by only about 6%, so a larger reduction would require additional flexible resources such as controllable loads or a stochastic EV schedule. Figure 8b shows in-sample values; out-of-sample means are given in Table 8.

4.5. Sensitivity Analyses

The proposed strategy ($\theta = 1\%$ unless stated) was tested for the ESS SOC window, power rating, EFC threshold, PV size and export, and grid-import limit (Table 10), and for the number of training scenarios and the uncertainty scale (Table 11). Values are changes in the out-of-sample mean against the static and the Adaptive Baseline of the same case. Table 10 and the uncertainty rows of Table 11 use one training seed (42), the training-scenario rows of Table 11 use three seeds, and all cases are evaluated on two test sets of 2000 scenarios (seeds 10,001 and 10,002), so the $N_s = 100$ row differs slightly from Tables 7 and 8. In Table 8, the seed-to-seed spread relative to the static Baseline is about 0.5 percentage points for the changes in cost, CVaR, and EFC (0.05, 0.17, and 0.49 relative

to the Adaptive Baseline), and the single-seed base case differs from the three-seed result accordingly; differences smaller than these spreads are not interpreted as effects.

ESS design. The cost increase relative to the Adaptive Baseline is practically constant (1.12–1.16%) for the SOC windows and power ratings tested. The cycling reduction grows as the usable SOC window narrows (−3.2%, −4.3%, and −6.7% for 10–90%, 20–80%, and 30–70%), whereas the power rating has almost no influence (−4.3% to −4.5%), consistent with the ESS rarely being at its power limit during curtailment (Table 9). Relative to the static Baseline, the cost change stays within ±0.12% and the CVaR reduction is between 1.6% and 2.0%.

EFC threshold. In place of the cost budget, the proposed strategy was re-solved with the EFC cap of Equation (32) computed with the ESS EFC of the Adaptive Baseline in place of F_B and the adaptive EFC reference of Table 6 in place of F_A, keeping the CVaR and EV-throughput constraints of Equation (35). Table 10 shows an almost linear trade-off for γ_D from 0.25 to 1: cycling falls by 2.2% to 9.2% for a cost increase of 0.59% to 2.67% (3.4–3.7% less cycling per 1% of additional cost), with a CVaR increase of at most 0.49% and, by Equation (35), no EV throughput above that of the Adaptive Baseline. The cycling reduction can therefore be set through a single parameter at a known cost.

PV size, export, and import limit. PV not used locally is the curtailed or exported share of the available PV energy (Table 10). Without export, PV sizes of 0.5 to 2 times the base size leave the cost increase relative to the Adaptive Baseline at 1.06–1.16% and the CVaR reduction relative to the static Baseline at 1.4–1.9%. The cycling reduction is largest for the small PV system (−8.1% for 0.5 times). An import limit of 80% or 60% of the unconstrained peak changes none of the indicators noticeably (Baseline cost +0.2% at 60%). When exported PV energy is remunerated at half the purchase tariff ($\kappa = 0.5$), the expected cost relative to the static Baseline rises by 0.9–1.0% and the CVaR reduction relative to the static Baseline disappears (+0.07% to −0.17%), while the cycling reduction remains (−1.0% to −15.3%) at 1.10–1.52% additional cost relative to the Adaptive Baseline. The CVaR advantage discussed in Section 4.3 is therefore tied to the no-export rule, under which PV forecast errors are curtailed and can be absorbed by the adaptive ESS; with export, the surplus has an outlet, an explanation that was not tested separately. The PV × 1.5 case with export has a Baseline cost close to zero (53.17 DKK/day), so its percentage changes are inflated, and larger PV sizes with export were not evaluated because the Baseline cost would become negative.

Training scenarios and uncertainty scale. For 25 to 400 training scenarios (N_s in Table 11), the cost increase relative to the Adaptive Baseline stays at 0.9–1.1%. With 200 and 400 scenarios, the CVaR reduction relative to the static Baseline increases to 2.7% (2.1% for 100 scenarios), and the CVaR relative to the Adaptive Baseline equals it within 0.02%. So the small CVaR increase of 0.14% with 100 scenarios is a sampling effect; the overfitting check of Section 4.3 shows no sign of overfitting to the training scenarios. Scaling the standard deviations of the PV and load errors by a factor $\sigma = 0.5$, 1, 1.5, and 2 changes the CVaR relative to the static Baseline by −0.7%, −1.8%, −2.0%, and −2.6% and the expected cost by +0.67%, 0.00%, −0.45%, and −0.70%, so the advantage of the adaptive recourse grows with the uncertainty: at low uncertainty it does not compensate for the 1.1% cost of the cycling reduction, whereas at high uncertainty it does.

4.6. Solver Accuracy, Scalability, and Limitations

All optimization problems were implemented in Python 3.12.6 in matrix form (NumPy and SciPy sparse matrices) and solved with Gurobi 12.0.2 through its Python interface (relative MIP gap tolerance 10^{-6}, time limit 900 s per solve, automatic thread allocation) on

a 64-bit Windows 11 Home computer with an AMD Ryzen 7 7730U processor and 16 GB of RAM.

Table 12 shows the effect of the relative MIP gap tolerance (5×10^{-3} to 10^{-6}) on the 24 solves required for the Baseline, CVaR, EFC, Adaptive Baseline, and Proposed ($\theta = 1\%$) strategies, including their reference solutions, for the first training seed.

Table 13 gives the model size and solution time for communities of three to 50 homes with 100 scenarios, and for 25 to 400 scenarios with 10 homes. Since the ESS and PV are aggregated at the community level, the number of variables grows slowly with the number of homes (5153 to 7625 static, 12,353 to 14,825 adaptive) and the total solution time remains between 42 and 52 s, whereas the number of scenarios has a much larger influence: with 10 homes the time increases from 5.4 s (25 scenarios) to 44.5 s (100), 136 s (200), and 545 s (400). The risk and EFC reference solves of the ε-constraint procedure require only 0.8–3.0% of the solution time, so the iterative reference step is not the source of the growth. The proposed strategy keeps an ESS EFC of 0.57–0.58 cycles/day in all settings (0.6 for the Baseline). The cost and CVaR per home decrease with community size, but this also reflects the synthetic composition of the added homes and is not interpreted as a pooling effect. The stochastic MILP remains practical for 24 h day-ahead scheduling across the investigated sizes.

Table 13. Model size, solution time, and results of the proposed strategy ($\theta = 1\%$) for different community sizes and scenario numbers (first training seed). Binary counts refer to this single-binary implementation.

Setting (Homes, Scenarios)	Variables, Static Model (Binary)	Variables, Adaptive Model (Binary)	Total Solver Time (s)	Time in Reference Solves (%)	Expected Cost per Home (DKK/Day)	$CVaR_{0.90}$ per Home (DKK/Day)	ESS EFC, Proposed (Cycles/Day)
3, 100	5153 (63)	12,353 (39)	44.3	1.1	65.2	71.5	0.569
5, 100	5261 (90)	12,461 (66)	42.4	1.1	55.8	62.0	0.572
10, 100	5529 (157)	12,729 (133)	44.5	1.3	52.8	59.0	0.575
20, 100	6037 (284)	13,237 (260)	42.5	1.8	51.5	57.4	0.574
50, 100	7625 (681)	14,825 (657)	52.1	2.9	50.2	56.0	0.575
10, 25	1854 (157)	3654 (133)	5.4	3.0	52.7	59.6	0.580
10, 50	3079 (157)	6679 (133)	16.6	1.9	52.7	58.9	0.577
10, 200	10,429 (157)	24,829 (133)	136.1	2.5	52.8	59.0	0.574
10, 400	20,229 (157)	49,029 (133)	544.9	0.8	52.9	59.0	0.575

Load data and limitations. Measured household loads are available for ten homes; the communities of 20 and 50 homes were generated by scaling and circularly shifting measured profiles, which serves only the assessment of computation time and of the persistence of the cycling reduction. Table 14 shows that the synthetic households agree with the measured ones in daily energy, peak power, load factor, evening share, and EV arrival and departure hours, but their correlation with the mean measured profile is lower (0.43 vs. 0.61) because the shifted profiles no longer follow the common daily pattern. The results for more than ten homes are therefore valid for computation time and the order of magnitude of the cycling reduction, not for the economics of a larger community. The economic evaluation is also limited to a ten-home community with one tariff, one climate, and one PV and load data set, so absolute cost values cannot be transferred to other systems. The model also has no feeder-level network representation, so limits on reverse power flow and voltage on the distribution-network side are not considered; only the aggregate grid-import limit and the export option of Section 3.3 were examined.

Table 14. Statistics of measured and synthetic household loads and EV connection hours (mean ± standard deviation over homes).

Quantity	Measured	Synthetic
Daily energy, scaled measured (kWh/day)	28.800 ± 0.000	27.834 ± 2.589
Peak power (kW)	2.673 ± 0.888	2.592 ± 0.894
Load factor	0.494 ± 0.154	0.494 ± 0.148
Evening share (18–22 h)	0.260 ± 0.053	0.252 ± 0.070
Correlation with the measured mean profile	0.610 ± 0.307	0.432 ± 0.296
EV arrival hour	18.500 ± 1.080	18.725 ± 1.219
EV departure hour	7.800 ± 1.033	7.825 ± 1.196

5. Conclusions

This study developed a stochastic MILP framework for centralized multi-home energy management with equivalent aggregated PV and ESS resources and household EVs. It integrates CVaR-based risk management and EFC-based control of shared-ESS cycling-related degradation under PV and load uncertainties, using an ε-constraint formulation and a causal-adaptive ESS dispatch.

Benchmark reproduction yielded a cost of 288.25 DKK/day against the published 287.50 DKK/day (0.26% error). On independent test scenarios, the proposed strategy ($\theta = 1\%$) lowered expected cost by 0.24%, $CVaR_{0.90}$ by 2.18%, and ESS EFC by 4.37% relative to the static Baseline; with $\theta = 2\%$, ESS EFC fell by 8.21% at a 0.85% higher cost. Relative to the Adaptive Baseline, it reduced the ESS EFC by 4.46% for a 1.12% cost increase at practically unchanged CVaR and EV throughput. The CVaR reduction stems from the adaptive recourse, not from the constraints, and depends on the no-export rule. Including wear costs, the proposed strategy is cheaper than the static Baseline but not cheaper than the Adaptive Baseline at present battery prices. Scalability tests from 3 to 50 homes showed nearly constant ESS EFC and computationally practical 24 h day-ahead scheduling.

The main limitations are that EFC is used as a throughput-based proxy for ESS degradation, that the EV schedule is fixed day ahead, that the CVaR advantage depends on the no-export rule with no feeder-level network represented, and that the 20- and 50-home cases rely on synthetic profile extensions. Future work will consider more detailed degradation modeling, adaptive EV scheduling, and rolling-horizon implementation.

Author Contributions: Conceptualization, A.K. and C.S.; methodology, A.K.; software, A.K.; validation, A.K., A.N., M.N. and N.B.; formal analysis, A.K.; investigation, A.K., A.N., M.N. and N.B.; data curation, A.K.; writing—original draft preparation, A.K.; writing—review and editing, A.N., M.N., N.B., C.S., N.A. and A.S.; visualization, A.K.; supervision, C.S. and N.A.; project administration, C.S. and N.A. All authors have read and agreed to the published version of the manuscript.

Funding: This research received no external funding.

Data Availability Statement: The data presented in this study are available on request from the corresponding author. The data are not publicly available due to the privacy requirements of data owners.

Acknowledgments: The authors gratefully acknowledge the Center of Multidisciplinary Innovation Network Talent (MINT Center), Faculty of Interdisciplinary Studies, Khon Kaen University, Nong Khai Campus, for providing access to the database and research facilities that supported this study. During the preparation of this manuscript/study, the authors used ChatGPT (GPT-5.6, OpenAI) for the purposes of generating selected graphical elements in Figure 1, specifically the illustrations of the photovoltaic (PV) system, energy storage system (ESS), and residential house. The authors designed and prepared the overall system architecture, figure layout, labels, arrows, power and data flows, and technical content of Figure 1. The authors have reviewed and edited the output and take full responsibility for the content of this publication.

Conflicts of Interest: The authors declare no conflicts of interest.

Abbreviations

The following abbreviations are used in this manuscript:

AR(1)	First-Order Autoregressive Model
BNEF	BloombergNEF
VaR	Value-at-Risk
CVaR	Conditional Value-at-Risk
DKK	Danish Krone
DoD	Depth of Discharge
DRL	Deep Reinforcement Learning
EFC	Equivalent Full Cycle
EMS	Energy Management System
ESS	Energy Storage System
EV	Electric Vehicle
HEMS	Home Energy Management System
LFP	Lithium Iron Phosphate
MILP	Mixed-Integer Linear Programming
PV	Photovoltaic
RTP	Real-Time Pricing
SH	Smart Home
SOC	State of Charge
V2H	Vehicle-to-Home

References

1. Das, N.; Haque, A.; Zaman, H.; Morsalin, S.; Islam, S. Domestic Load Management With Coordinated Photovoltaics, Battery Storage and Electric Vehicle Operation. *IEEE Access* **2023**, *11*, 12075–12087. [CrossRef]
2. Zhang, C.; Yi, X.; Liao, Q. Demand-Side Management for Smart Homes with Battery Energy Storage Systems and Electric Vehicles Integration under Day-Ahead Pricing. *J. Energy Storage* **2026**, *160*, 121782. [CrossRef]
3. Faia, R.; Faria, P.; Vale, Z. Optimal Energy Management with Discomfort Calculation in Residential Buildings Considering Load Shifting and Home Battery Storage System. *Sustain. Energy Grids Netw.* **2025**, *41*, 101624. [CrossRef]
4. Chatterjee, A.; Paul, S.; Ganguly, B. Multi-Objective Energy Management of a Smart Home in Real Time Environment. *IEEE Trans. Ind. Appl.* **2023**, *59*, 138–147. [CrossRef]
5. Prum, P.; Charoen, P.; Khan, M.A.; Bayati, N.; Charoenlarpnopparut, C. Energy Management Scheme for Optimizing Multiple Smart Homes Equipped with Electric Vehicles. *Energies* **2024**, *17*, 254. [CrossRef]
6. Almughram, O.; Ben Slama, S.; Zafar, B. Model for Managing the Integration of a Vehicle-to-Home Unit into an Intelligent Home Energy Management System. *Sensors* **2022**, *22*, 8142. [CrossRef] [PubMed]
7. GhasemiGarpachi, M.; Dehghani, M.; Aly, M.; Rodriguez, J. Multi-Objective Improved Differential Evolution Algorithm-Based Smart Home Energy Management System Considering Energy Storage System, Photovoltaic, and Electric Vehicle. *IEEE Access* **2025**, *13*, 89946–89966. [CrossRef]
8. Xiong, S.; Liu, D.; Chen, Y.; Zhang, Y.; Cai, X. A Deep Reinforcement Learning Approach Based Energy Management Strategy for Home Energy System Considering the Time-of-Use Price and Real-Time Control of Energy Storage System. *Energy Rep.* **2024**, *11*, 3501–3508. [CrossRef]
9. Yuan, J.; Zeng, X.; Zhou, J.; Li, J.; Lv, J.; Chen, R.; Chen, K.; Yang, W.; Zhang, Y. Data-Driven Real-Time Home Energy Management System Based on Adaptive Dynamic Programming. *Electr. Power Syst. Res.* **2025**, *238*, 111055. [CrossRef]
10. Ren, K.; Liu, J.; Wu, Z.; Liu, X.; Nie, Y.; Xu, H. A Data-Driven DRL-Based Home Energy Management System Optimization Framework Considering Uncertain Household Parameters. *Appl. Energy* **2024**, *355*, 122258. [CrossRef]
11. Felicetti, R.; Ferracuti, F.; Iarlori, S.; Monteriù, A. Peak Shaving and Self-Consumption Maximization in Home Energy Management Systems: A Combined Integer Programming and Reinforcement Learning Approach. *Comput. Electr. Eng.* **2024**, *117*, 109283. [CrossRef]
12. Saber, H.; Ehsan, M.; Moeini-Aghtaie, M.; Fotuhi-Firuzabad, M.; Lehtonen, M. Distributed Transactive Coordination of Residential Communities Aiming at Fulfilling Households' Preferences. *IEEE Access* **2022**, *10*, 122010–122021. [CrossRef]
13. Cerna, F.V.; Pourakbari-Kasmaei, M.; Barros, R.G.; Naderi, E.; Lehtonen, M.; Contreras, J. Optimal Operating Scheme of Neighborhood Energy Storage Communities to Improve Power Grid Performance in Smart Cities. *Appl. Energy* **2023**, *331*, 120411. [CrossRef]

14. Nishanthy, J.; Raja, S.C.; Nesamalar, J.J.D. Feasibility Analysis of Solar PV System in Presence of EV Charging with Transactive Energy Management for a Community-Based Residential System. *Energy Convers. Manag.* **2023**, *288*, 117125. [CrossRef]
15. Görgülü, H.; Topçuoğlu, Y.; Yaldız, A.; Gökçek, T.; Ateş, Y.; Erdinç, O. Peer-to-Peer Energy Trading among Smart Homes Considering Responsive Demand and Interactive Visual Interface for Monitoring. *Sustain. Energy Grids Netw.* **2022**, *29*, 100584. [CrossRef]
16. Abbasi, A.; Sultan, K.; Afsar, S.; Aziz, M.A.; Khalid, H.A. Optimal Demand Response Using Battery Storage Systems and Electric Vehicles in Community Home Energy Management System-Based Microgrids. *Energies* **2023**, *16*, 5024. [CrossRef]
17. Huang, P.; Munkhammar, J.; Fachrizal, R.; Lovati, M.; Zhang, X.; Sun, Y. Comparative Studies of EV Fleet Smart Charging Approaches for Demand Response in Solar-Powered Building Communities. *Sustain. Cities Soc.* **2022**, *85*, 104094. [CrossRef]
18. Beyazıt, M.A.; Taşcıkaraoğlu, A.; Catalão, J.P.S. Cost Optimization of a Microgrid Considering Vehicle-to-Grid Technology and Demand Response. *Sustain. Energy Grids Netw.* **2022**, *32*, 100924. [CrossRef]
19. Etedadi, F.; Danté, A.W.; Kelouwani, S.; Henao, N.; Agbossou, K.; Fournier, M. Distributed Coordination of Electric Vehicles Charging Station and Home Energy Management Systems in Residential Neighborhood. *Int. J. Electr. Power Energy Syst.* **2025**, *172*, 111142. [CrossRef]
20. Kaewdornhan, N.; Srithapon, C.; Liemthong, R.; Chatthaworn, R. Real-Time Multi-Home Energy Management with EV Charging Scheduling Using Multi-Agent Deep Reinforcement Learning Optimization. *Energies* **2023**, *16*, 2357. [CrossRef]
21. Mohammadi, F.; Faghihi, F.; Kazemi, A.; Salemi, A.H. The Effect of Multi-Uncertainties on Battery Energy Storage System Sizing in Smart Homes. *J. Energy Storage* **2022**, *52*, 104765. [CrossRef]
22. Gil-González, W.; Montoya, O.D.; Cortés-Caicedo, B. Stochastic Home Energy Management While Considering the Shifting of Electric Appliances, Solar Energy, and Battery Systems. *J. Energy Storage* **2026**, *153*, 120858. [CrossRef]
23. Zaytoun, A.M.; Abdul Maksoud, I.A.; Rabia, S.I. Multi-Objective Home Energy Management System with Realistic Load Classification and Multi-Source Uncertainty Modeling: A Robust Optimization Approach. *J. Process Control* **2026**, *162*, 103722. [CrossRef]
24. Karimianfard, H. A Robust Optimization Framework for Smart Home Energy Management: Integrating Photovoltaic Storage, Electric Vehicle Charging, and Demand Response. *J. Energy Storage* **2025**, *110*, 115259. [CrossRef]
25. Kanakadhurga, D.; Prabaharan, N. Smart Home Energy Management Using Demand Response with Uncertainty Analysis of Electric Vehicle in the Presence of Renewable Energy Sources. *Appl. Energy* **2024**, *364*, 123062. [CrossRef]
26. Javadi, M.S.; Nezhad, A.E.; Gough, M.; Lotfi, M.; Anvari-Moghaddam, A.; Nardelli, P.H.J.; Sahoo, S.; Catalão, J.P.S. Conditional Value-at-Risk Model for Smart Home Energy Management Systems. *e-Prime Adv. Electr. Eng. Electron. Energy* **2021**, *1*, 100006. [CrossRef]
27. Zhang, C.; Liang, H.; Yang, L. A Distributionally Robust Approximate Framework Consider CVaR Constraints for Energy Management of Microgrid. *Sustain. Energy Grids Netw.* **2023**, *36*, 101172. [CrossRef]
28. He, S.; Gao, H.; Tang, Z.; Chen, Z.; Jin, X.; Liu, J. Worst CVaR Based Energy Management for Generalized Energy Storage Enabled Building-Integrated Energy Systems. *Renew. Energy* **2023**, *203*, 255–266. [CrossRef]
29. Yaseen, M.; Nizami, I.F.; Aldajani, M.B.; Raja, A.A.; Haroon, F.; Abbas, Q. Resilient Constraint Energy Management for Microgrids: Integrating Wasserstein DRO and CVaR-Constrained MPC Under Renewable Uncertainty. *IEEE Access* **2026**, *14*, 11534–11559. [CrossRef]
30. Merrington, S.; Khezri, R.; Mahmoudi, A. Optimal Sizing of Grid-Connected Rooftop Photovoltaic and Battery Energy Storage for Houses with Electric Vehicle. *IET Smart Grid* **2023**, *6*, 297–311. [CrossRef]
31. Minhas, D.M.; Meiers, J.; Frey, G. Electric Vehicle Battery Storage Concentric Intelligent Home Energy Management System Using Real Life Data Sets. *Energies* **2022**, *15*, 1619. [CrossRef]
32. Dehghani, M.; Bornapour, S.M.; Ruiz, F.; Rodriguez, J. Multi-Objective Energy Management System in Smart Homes with Inverter-Based Air Conditioner Considering Costs, Peak-Average Ratio, and Battery Discharging Cycles of ESS and EV. *Energies* **2025**, *18*, 5298. [CrossRef]
33. Al Muala, Z.A.; Bany Issa, M.A.; Sansó-Rubert Pascual, D.; Bello Bugallo, P.M. Realistic Home Energy Management System Considering the Life Cycle of Photovoltaic and Energy Storage Systems. *Sustainability* **2023**, *15*, 11205. [CrossRef]
34. Sasanmoghadam, S.; Sabri-Laghaie, K. Adaptive Scheduling and Storage System Preservation in Smart Home Energy Management Systems: Considering Cost Efficiency, User Satisfaction and Storage Systems Durability. *J. Energy Storage* **2026**, *142*, 119521. [CrossRef]
35. Dias de Lima, T.; Faria, P.; Vale, Z. Optimizing Home Energy Management Systems: A Mixed Integer Linear Programming Model Considering Battery Cycle Degradation. *Energy Build.* **2025**, *329*, 115251. [CrossRef]
36. IEEE Power & Energy Society. IEEE Open Data Sets. Available online: https://site.ieee.org/pes-iss/data-sets/#cons (accessed on 7 May 2026).
37. Rockafellar, R.T.; Uryasev, S. Optimization of Conditional Value-at-Risk. *J. Risk* **2000**, *2*, 21–41. [CrossRef]

38. Ben-Tal, A.; Goryashko, A.; Guslitzer, E.; Nemirovski, A. Adjustable Robust Solutions of Uncertain Linear Programs. *Math. Program.* **2004**, *99*, 351–376. [CrossRef]
39. Colthorpe, A. Battery Storage System Prices Continue to Fall Sharply, BNEF and Ember Reports Find. 2025. Available online: https://www.energy-storage.news/?p=92133 (accessed on 12 October 2026).
40. Danish Energy Agency; Energinet. Technology Data—Energy Storage, Chapter 180: Lithium-Ion Batteries for Grid-Scale Storage, Version 0011; Danish Energy Agency: Copenhagen, Denmark, 2018 (chapter updated May 2025). Available online: https://ens.dk/en/analyses-and-statistics/technology-data-energy-storage (accessed on 12 October 2026).
41. U.S. Department of Energy, Office of Electricity. *Lithium-ion Batteries Technology Strategy Assessment*; Report DOE/OE-0031; U.S. Department of Energy: Washington, DC, USA, 2023. Available online: https://www.energy.gov/sites/default/files/2023-09/2_Technology%20Strategy%20Assessment%20-%202%20Lithium-ion_508.pdf (accessed on 12 October 2026).
42. BloombergNEF. *Lithium-Ion Battery Pack Prices Fall to $108 per Kilowatt-Hour, Despite Rising Metal Prices*; Press Release; BloombergNEF: New York, NY, USA, 2025. Available online: https://about.bnef.com/insights/clean-energy/lithium-ion-battery-pack-prices-fall-to-108-per-kilowatt-hour (accessed on 12 October 2026).

Disclaimer/Publisher's Note: The statements, opinions and data contained in all publications are solely those of the individual author(s) and contributor(s) and not of MDPI and/or the editor(s). MDPI and/or the editor(s) disclaim responsibility for any injury to people or property resulting from any ideas, methods, instructions or products referred to in the content.